8/1/95

SANDIA REPORT

SAND95-1064 • UC–1290
Unlimited Release
Printed June 1995

Test Report on the Abacus 30 kW Bimode® Inverter and Maximum Power Tracker

Russell Bonn, Jerry Ginn, Jeff Zirzow, Greg Sittler

Prepared by
Sandia National Laboratories
Albuquerque, New Mexico 87185 and Livermore, California 94550
for the United States Department of Energy
under Contract DE-AC04-94AL85000

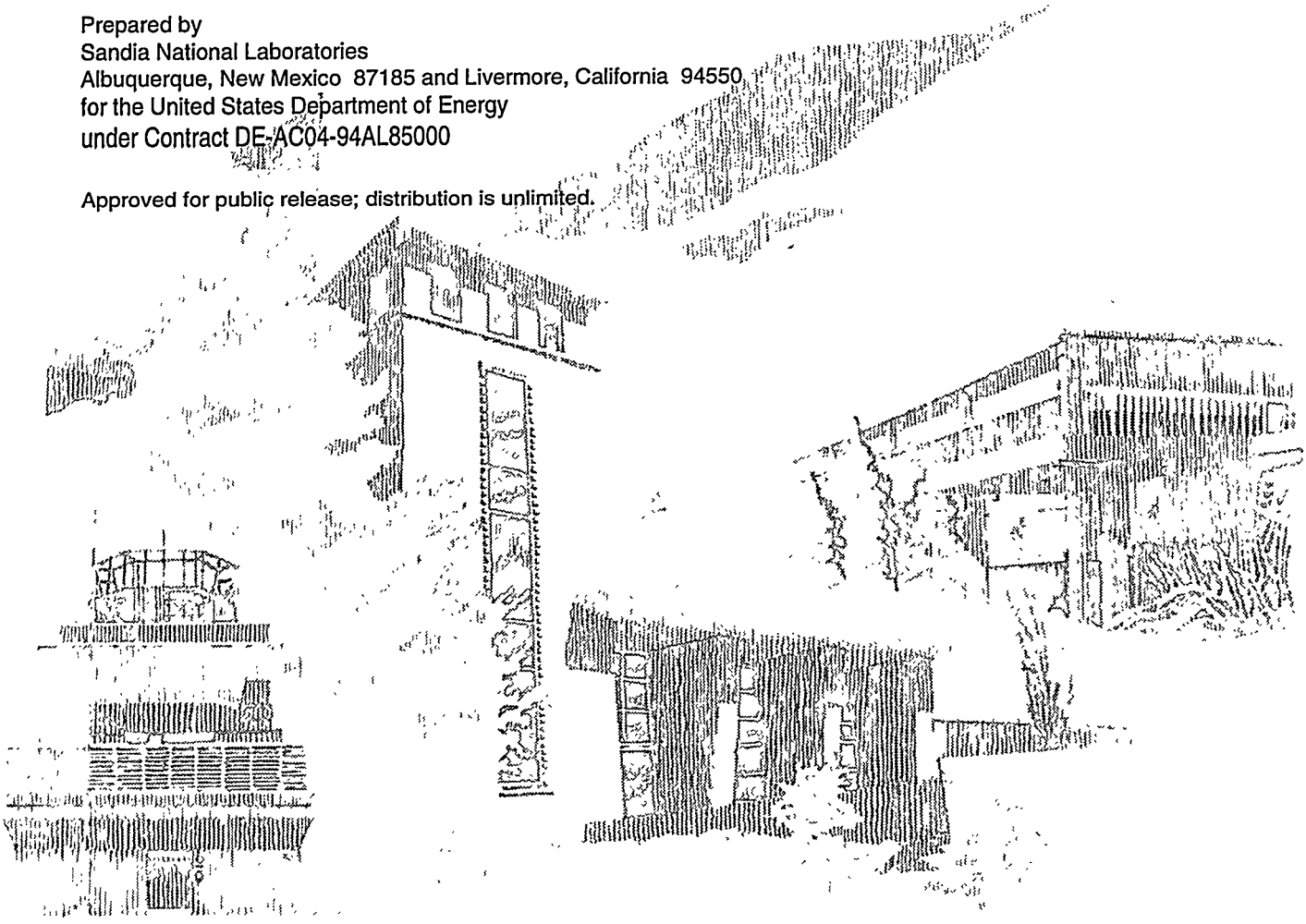

SF2900Q(8-81)

Issued by Sandia National Laboratories, operated for the United States Department of Energy by Sandia Corporation.

Available to DOE and DOE contractors from
Office of Scientific and Technical Information
PO Box 62
Oak Ridge, TN 37831

Prices available from (615) 576-8401, FTS 626-8401

Available to the public from
National Technical Information Service
US Department of Commerce
5285 Port Royal Rd
Springfield, VA 22161

NTIS price codes
Printed copy: A03
Microfiche copy:

DISCLAIMER

Portions of this document may be illegible electronic image products. Images are produced from the best available original document.

SAND95-1064
Unlimited Release
Printed June 1995

Test Report on the Abacus 30 kW Bimode® Inverter and Maximum Power Tracker (MPT)

Russell Bonn, Jerry Ginn, Jeff Zirzow, Greg Sittler
Photovoltaics Systems Applications Department
Sandia National Laboratories
Albuquerque, NM, 87185-5800

Abstract

Sandia National Laboratories conducts the photovoltaic balance of systems (BOS) program, which is sponsored by the US Department of Energy's Office of Energy Management. Under this program, SNL lets commercialization contracts and conducts a laboratory program designed to advance BOS technology, improve BOS component reliability, and reduce the BOS life-cycle-cost. This report details the testing of the first large US manufactured hybrid inverter and its associated maximum power tracker.

Table of Contents

Figures

tc

Charts

Tables

Test Report on the Abacus 30 kW Bimode® Inverter and Maximum Power Tracker (MPT)

1. Executive Overview

Some of Sandia's recent work with renewable energy systems has focused on developing large hybrid systems, those greater than 10 kW. The primary impetus came from the Department of Defense Strategic Environmental Research Development Plan (SERDP), which is responsible for installing photovoltaic hybrid systems on military facilities. When the plan began, there were no hybrid inverters made by U.S. manufacturers; Sandia's role has included both developmental contracts and laboratory testing of inverters made by U.S. industry. This report documents Sandia's tests of the first hybrid inverter and maximum power tracker made in the United States and serves as a method for evaluating hybrid photovoltaic systems.

The results of our tests on the Abacus Controls, Inc., bimode® inverter and its maximum power tracker (MPT) are reported here. The tests are designed to evaluate the manufacturer's specifications and to apply typical electrical stresses anticipated in normal field use. They include some system testing, combining a battery string of four 48-volt batteries (192 Vdc), a photovoltaic array of 25 kW, the maximum power tracker, and the inverter to simulate a small village power system, as shown in the sketch bellow. Our intent is to evaluate all parameters important to a potential user; many have never before been thoroughly characterized in hybrid photovoltaic systems. This is the first in a series of tests, which includes inverters from Omnion and AES.

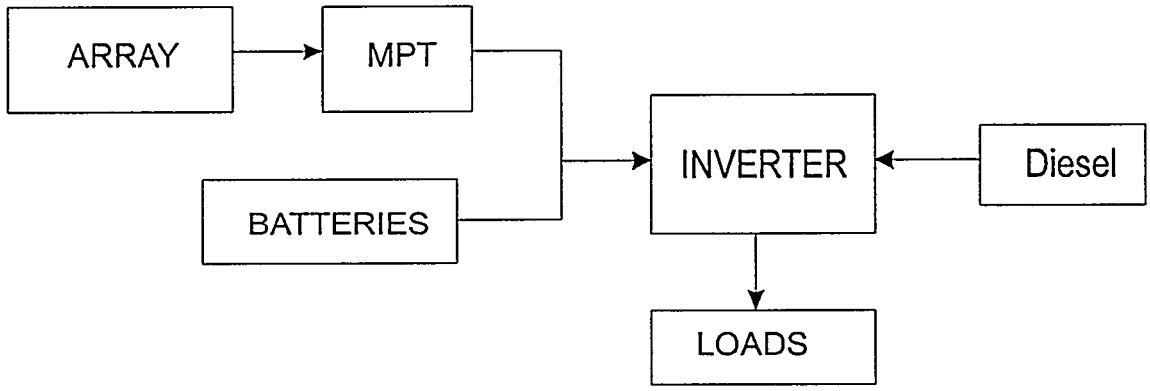

Inverter and MPT configured as a System

The evaluations are designed to

1. confirm that the hardware meets the manufacturer's specifications,
2. quantify additional parameters that may be important to the user
3. identify problems with the system operations.

For parameters that are undefined, the real criterion is that the hybrid system not have a worse performance than the alternative diesel generator system. For that reason, test results are frequently compared with the same load or condition placed on a diesel or on the Sandia grid.

The results of our tests on the Abacus inverter demonstrated that it was able to handle its rated capacity, reactive and nonlinear loads, and transient surges such as motor starts, in a manner comparable to a diesel generator. The typical efficiency was

91% for resistive loads greater than 50% of rated power. Voltage distortion was less than the specified value of 2% for resistive loads between zero and rated power. The battery charging efficiency was approximately 89.5% for full charging current. The built-in system controls operated as advertised, and the battery charge/discharge control algorithm was successful. Finally, the efficiency of the MPT ranged from 96.7 to 99.4%.

1.1 System Overview

This is a test report for the Abacus Controls Inc. 30 kW bimode® inverter and maximum power tracker. The Abacus inverter (Model 639-4-RA) and the Abacus MPT 240 maximum power tracker were configured as components in a simulated hybrid photovoltaics system which included a diesel generator, a photovoltaic array, and a battery bank.; the SNL diesel is a 75 kW KAMAG, Model # 75SC9E manufactured by Reliance Electric Co.

The Abacus bimode® power processor is comprised of a power processing controller, an inverter, and a battery charger. A 25 kW dc-to-dc maximum power tracker was included as a part of the system. These system elements are described below.

Maximum Power Tracker: The MPT converts power from a photovoltaic array to a battery hybrid power center. The photovoltaic array is operated at its maximum power point, while the battery accepts a charge current at its present operating voltage. Power conversion changes to constant voltage when the battery reaches its float voltage.

Power Processing Controller: The PPC optimizes the use of photovoltaic energy and reduces the consumption of diesel fuel by determining when the diesel engine generator will supply the ac load and when the inverter will supply the ac load.

Battery Charger: The battery charger uses the same bridges that the inverter uses. The use of the bridges for transferring power in both directions is trademarked as bimode® inverter operation by Abacus Controls Inc. The battery charger is specified to draw a unity power factor current from any ac source. In a three phase system, each phase draws power independent of the other phases.

Inverter: Three nearly identical inverters supply power to the three ac phases. One of the inverters functions as a master and the other two as slaves. The inverter has a nominal input voltage of 200 Vdc and a nominal output voltage of 277 Vac. With the diesel engine generator on, each inverter phase locks to its corresponding incoming phase. When the diesel power is not available, the phase A inverter free runs at 60 Hz and digitally creates phase references at 120° and 240° for the phase lock circuits in the other inverters.

2. Objectives

The objectives of this test were to evaluate the Abacus bimode® inverter and Abacus maximum power tracker (MPT) and to document a method for performing an evaluation of a hybrid, photovoltaic system. The testing included some system testing which combined a battery string of four 48 volt batteries (192 Vdc), a PV array of 25 kW, the MPT, and the inverter to simulate a small village power system.

3. Testing

3.1 Overview of Tests

The tests were designed to evaluate the manufacturer's specifications (Abacus performance criteria) and to apply typical electrical stresses that are anticipated in normal field usage (additional evaluation parameters). The parameters that were evaluated are listed in Table 1. The test plan (TP) paragraph that describes the test is listed next to each measured parameter. Those parameters that are included by Abacus as design parameters are included in the top portion of the table. Additional parameters, which SNL chose to evaluate, are included in the bottom portion of the table. Each element of Table 1 is then associated with a test. The major factor in considering test time was the battery state of charge. It is time consuming to go from full charge to low state-of-charge (SOC) on consecutive tests. Thus the test was ordered to minimize this. All tests were conducted at room temperature. The test plan, which is a separate document, can be obtained from SNL.

TP Para	Parameter/function evaluated
Abacus performance criteria	
ac output	
4.2.3.1	inverter rated power per phase 10 kVA continuous 12 kVA up to 30 minutes 17 kVA up to 10 minutes
4.2.1	voltage regulation, 277 V ac ±2%
4.2.1	total harmonic distortion (voltage) 2%
4.2.3.3	peak current, 86.6 A (instantaneous)
4.2.4.2.1	transfer voltage, 249 Vac (low line)
dc input	
4.2.4.1.2	full generator utilization
4.2.4.1.1	disconnect voltage = 168 Vdc
4.2.2.2	recharge current, 40 amps /phase maximum
4.2.4.1.1	float voltage, 216 Vdc generator start voltage, 175 Vdc
Additional Evaluation Parameters	
4.2.1	total distortion
4.2.3.3	surge power
4.2.3.2	transient & nonlinear loading
4.2.2	tare power
4.2.2.1	inverter efficiency
4.2.2.2	charger efficiency
4.2.2.3	battery efficiency
4.2.1	frequency stability
4.2.5.2 4.2.5.1	radiated emissions acoustic RFI
Maximum Power Tracker	
4.2.7.1	efficiency
4.2.7.4	dc operation range
4.2.7.2	benefit assessment
4.2.7.3	effectiveness
4.2.7.5	transient surges

Table 1: Planned Test Parameters

3.1.1 Standard Test Conditions

For the purpose of this test, a fully loaded inverter is defined as 10 kVA/phase (30 kVA total) with the diesel generator disabled. The "nominal" dc battery voltage is 192 volts dc or 2 volts per cell. The actual battery voltage varies according to the battery state of charge and load current. Throughout this test "nominal" battery voltage refers to a battery that is near full charge.

For the purpose of most of the following tests, an acceptable state of charge is > 85% (i.e. not more than 15% of the charge has been removed). "Low battery voltage" is defined as 180 volts (1.88 volts/cell) with any type of load. This value was selected because the inverter is supposed to initiate battery charging at 175 volts dc and therefore, the battery should not fall below that value for normal operation. Because parameter characterization may vary as a function of the dc voltage, it is important to define dc voltage. Note that this particular inverter is comprised of three identical units configured for phases A, B, and C. Because the three phases are independent, it is only necessary to perform the detailed tests on phase A. In addition, much operational data was collected on all three phases. Also, because of the manner in which the test was configured, the tests that involve automatic switching of the ac resistive load, placed identical resistive loads on all three phases. Thus, if the test calls for a load of 2 kW of nonlinear load and 2 kW of resistive load on phase A, phases B and C were also loaded with 2 kilowatts of resistive load.

3.2 Detailed Test Results

The test matrix (see appendix A) describes each measurement. The location of the measurement, as shown on the one-line diagram (see D sized drawing, "Abacus Bimode® Test Plan"), is indicated by a number. A letter identifies the recording instrument. For example, channel 48 B is a measurement of the phase A voltage distortion.

A - National Instruments measurement system
B - audio analyzer
C - signal analyzer
D - chart recorder
E - digital storage oscilloscope.

The test parameters are defined in Appendix B. Note that total distortion (TD) is recorded instead of total harmonic distortion (THD). These numbers are identical unless the inverter is generating noise below 3,000 Hz and are believe to be identical for this test.

The use of a single instrument for two measurements results in a time separation of the acquisition of the two data points. In some instances (for example, efficiency measurements), this time separation of the data acquisition introduces error into the measurement. All instruments were within their calibration period and the accuracy of all instruments is better than 1%. For example, the accuracy of the Yokogawa Power Meter is .2% of the reading plus .2% of the range. For the Abacus test this results in an error of .4% for full power readings. Useful implementation of the data does not require accuracy greater than 1%. Therefore, for this test report, additional error analysis was not conducted. Redundant measurements were taken with different types of instrumentation to increase confidence in data. For example, the voltage was also measured with a voltmeter.

3.2.1 Performance across Maximum ac Load Transitions

The ac distortion, voltage regulation, and frequency regulation of the load were evaluated just before and just after large changes in the ac load. THD is specified to be ≤5% when the peak nonlinear current is less than the peak current at full resistive load. The ac voltage regulation is specified as 277± 2% Vac line-to-neutral. The frequency stability is specified as 60 ±.5 Hz for all required load conditions. The total distortion (TD) and steady-state frequency were measured using an audio analyzer. Note that since the audio analyzer makes two measurements, it must be triggered twice with different functions selected. The regulation measurements described in this paragraph were acquired just before and just after large load changes. These changes included

- transfer from no load to full load
- transfer from full load to no load
- transfer from no load to reactive load (8 kW, .8 pf, 10 kVA load)
- transfer from reactive load to no load (8 kW, .8 pf, 10 kVA load)

Steady state frequency and distortion measurements were made before and after the transients.

In addition, the total distortion, voltage amplitude and frequency were monitored during other tests and those data were reviewed to assist in compliance evaluation.

Test Configuration.

PV power = disconnected

loads = variable

diesel = off (inverter forced on)

battery SOC = nominal

Data

After the initial evaluation of the data from this test it was determined that the load current was distorted due to current limiting. **This resulted from loads which exceeded 10.1 kW/phase.** The excessive loading caused distortion which exceeded the unit specifications and is apparent in data in Chart 1. Subsequently, the current limit was raised from 36.5 amps rms (51 amps peak) to 51 amps rms (72 amps peak) to allow for short duration overloads. This software change resulted in lower distortion for small overloads. In spite of the system over-stress the inverter performed well. It is interesting to note (see lower half of Chart 2) that each phase of the inverter turns off at the current zero crossing. This reduces transients in the voltage. The data are separated into two tables (Tables 2 and 3) corresponding to the data acquired before the increase in current limiting and the data acquired after the change.

Table 2 includes data taken prior to the adjustment of the current limit. Table 2 contains a value for frequency, phase A voltage, and distortion acquired prior to and after each load adjustment. In addition, four strip chart records of voltage and current transients are provided. Note that two data points were taken just before and after each transition. The transition point is identified by noting the change in the phase A load volt-amperes. The load changes were the worst case for the inverter. In a practical situation, the load is unlikely to change from zero to full load; some small load will usually be on

the inverter. Having some load on the inverter is important, because increases in load power result in a drop of the dc voltage. After conducting these initial tests, it was decided to conduct a second set of tests (see Table 3) that included a load change of 867 watts to full load. This test series was conducted after the modification to increase current limiting.

Frequency stability variation for large changes in loads. The change in the load did not cause a significant frequency shift. The data in the table show that the phase A frequency varied from a low of 59.33 Hz to a high of 60.17 Hz. Thus the change in recorded frequency was 0.89 Hz, with a center frequency of 59.8 Hz. This frequency shift may be the result of temperature variations over a period of time.

Voltage stability variation for large changes in loads. During the current limited portion of the test, phase A voltage varied from a high of 278.4 volts to a low of 265 volts or a change of (278.4-265)/277 = 4.8%, or a maximum change of 4.3% from a nominal voltage of 277 Vac. Because the inverter was in current limiting during this portion of the test, this number is not significant. It was noted that the dc voltage also varied significantly (by up to 11 volts). This is because the battery voltage at zero load is higher than the battery voltage with even a slight load. After the software modification, additional data were recorded. The load was changed from 1 kW to full load. When this test was performed and the voltage then varied from a high of 276.76 volts to a low of 272.75 volts or a change of (276.76-272.75)/277 = 1.4%.

Voltage distortion variation for large changes in loads. The maximum voltage total distortion observed after modification of the current limit value was 0.4%. This total distortion level occurred for a resistive load of 10 kW. The value of total distortion is unrelated to the transient associated with a change in load impedance.

System transient response during load transfer. The measured quantity is the result of the **system response**, not just the inverter response. The system includes a relay. Much of the observed distortion during the transfer to large loads may be attributed to relay chatter and not inverter response. Note the much cleaner response (Chart 2) when the relay is opened and no chatter exists.

Table 2: Distortion and voltage/ frequency regulation tests for linear loads before modification for current limiting

Load ON transition, Resistive Loads, Nominal Battery Voltage								
V_{bat}	% V_{dc} change	V_{la}	% V_{ac} change	VA	pf_A	AC Freq Hz	Δ freq Hz	% ACV Dist.
202.94		275.69		0.0	0.0	59.4		1.20
203.08		275.69		0.0	0.0	59.4		1.20
194.29	4.33%	264.99	3.88%	10352	1.00	59.3	.1	3.88
192.88		265.01		10371	1.00	59.3		3.91
Load OFF transition, Resistive Loads, Nominal Battery Voltage								
191.14		270.40		10348	1.00	59.4		2.55
190.84		270.48		10364	1.00	59.4		2.55
198.62	4.08%	276.16	2.10%	0.00	0.0	59.5	.1	1.16
199.46		276.11		0.00	0.0	59.5		1.16
Load ON transition, Reactive Loads, Nominal Battery Voltage								
213.00		276.63		0	1.000	60.1		1.100
211.25		276.74		0	1.000	60.1		1.097
205.31	2.81%	268.83	2.86%	10189	0.817	60.0	.1	2.148
202.57		269.19		10180	0.818	60.0		2.141
Load ON transition, Resistive Loads, Low Battery Voltage								
187.48		276.79		0	0	59.62		1.17
187.58		276.79		0	0	59.62		1.17
178.14	5.03%	278.47	0.61%	10131	1.00	59.62	.00	1.61
177.83		278.43		10126	1.00	59.61		1.58
Load OFF transition, Resistive Loads, Low Battery Voltage								
177.27		278.36		10112	1.00	59.6		1.59
177.19		278.33		10116	1.00	59.6		1.58
185.95	4.94%	276.76	0.56%	0	0	59.6	.0	1.18
186.93		276.72		0	0	59.6		1.18

Table 3: Distortion and voltage/ frequency regulation tests for linear loads after modification for current limiting

Load ON transition, Resistive Loads (1 kW to 10 kW), Nominal Battery Voltage								
V_{bat}	% V_{dc} change	V_{la}	% V_{ac} change	VA	pf_A	AC Freq Hz	Δ freq Hz	% ACV Dist.
205.96		272.75		867	.99	60.2		1.12
205.96		272.75		867	.99	60.2		1.13
195.47	1.4	276.76	1.44	10118	1.00	60.2	.0	1.17
191.58		277.12		10128	1.00	60.2		1.19

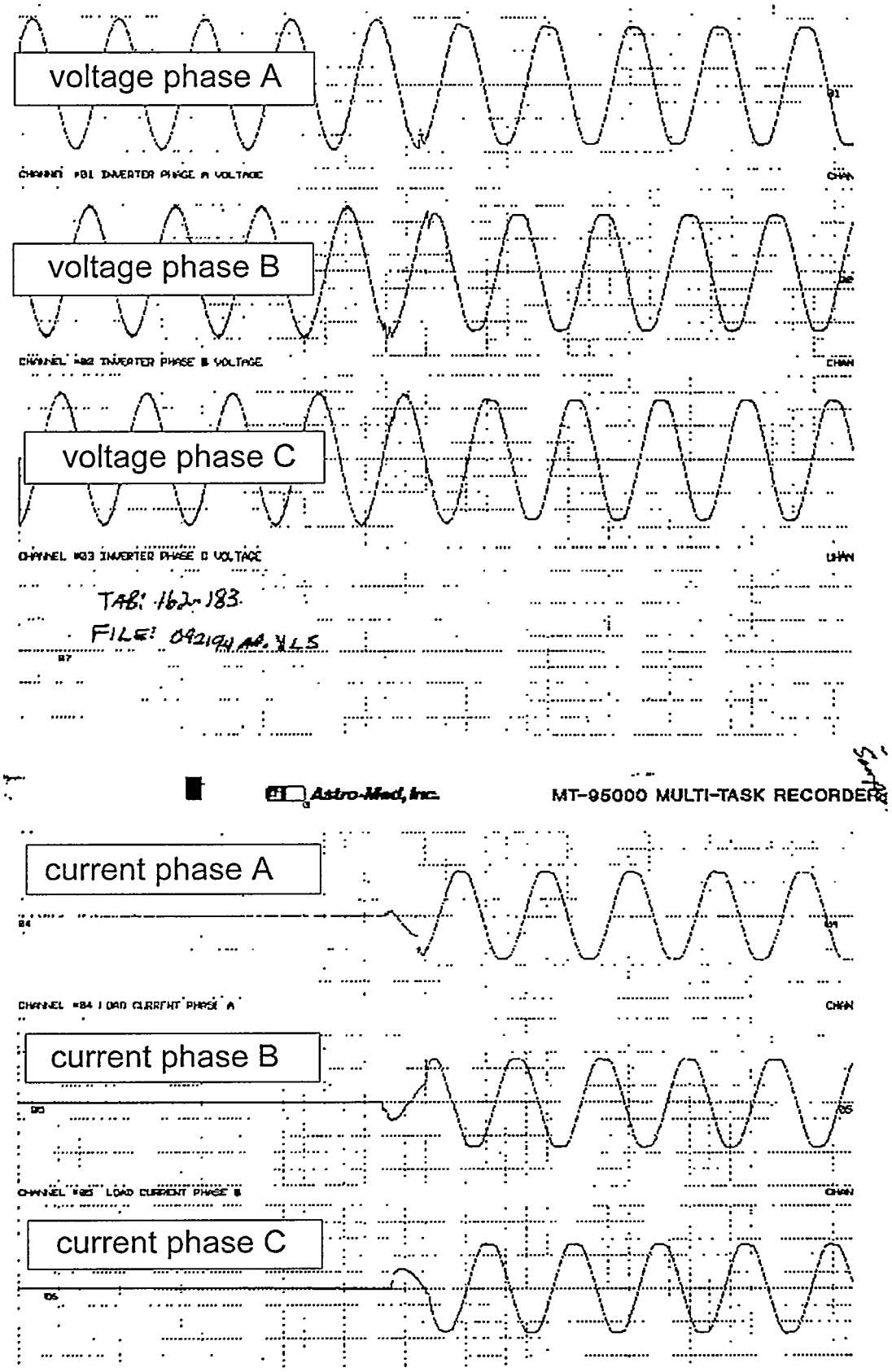

Chart 1: Transfer from no load to 10 kW resistive load

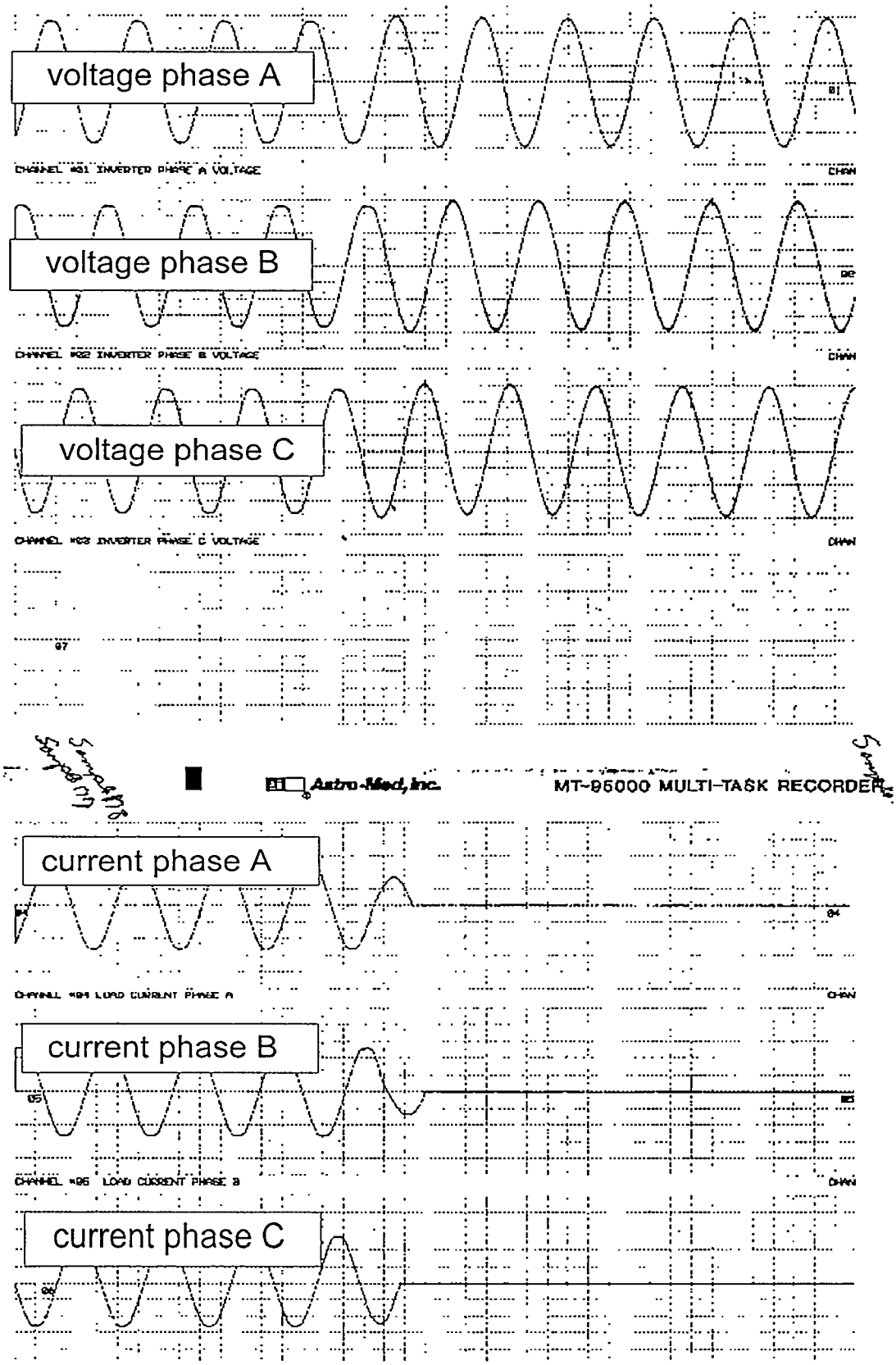

Chart 2: Transfer from 10 kW resistive load to no load

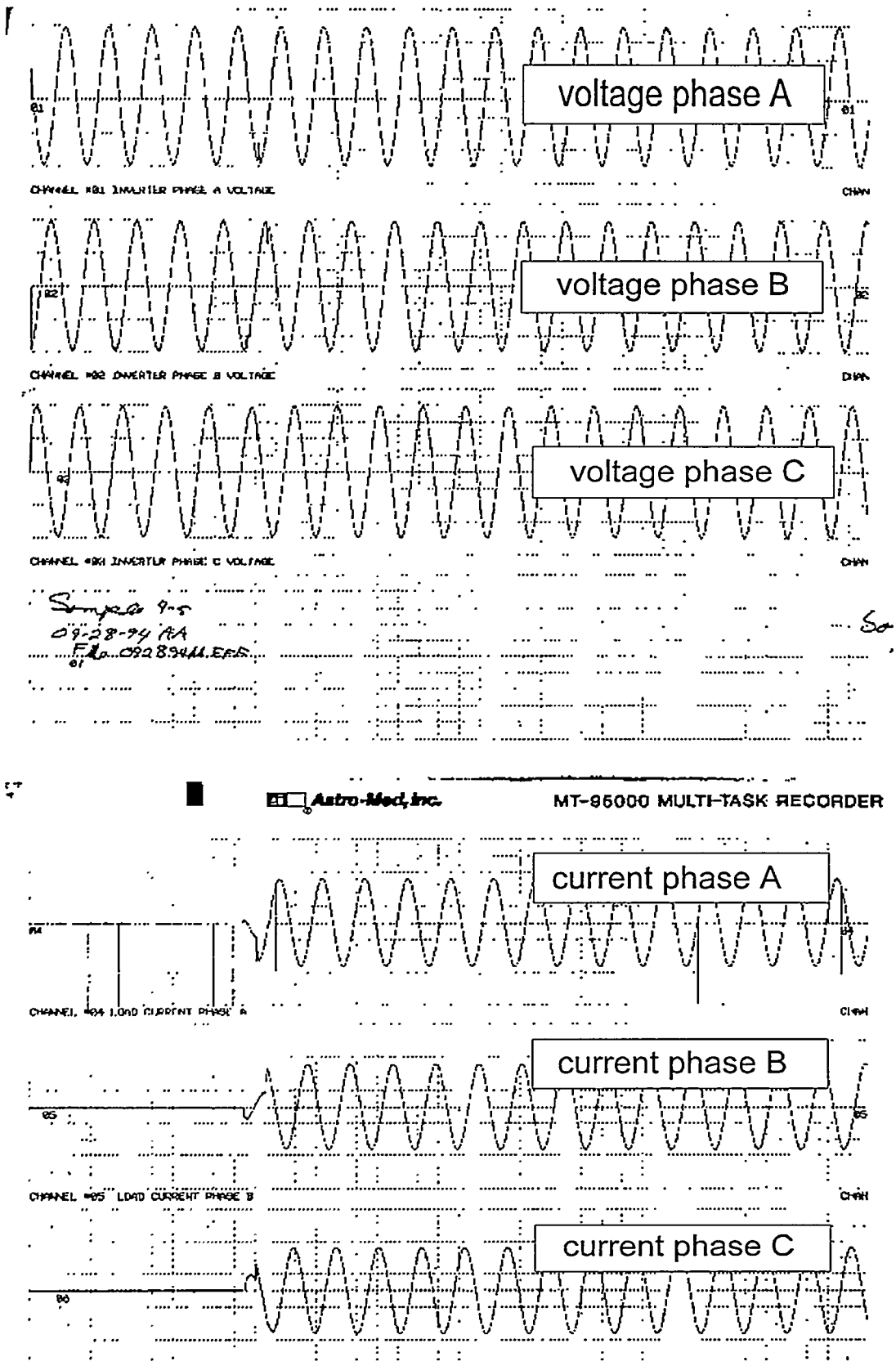

Chart 3: Transfer from no load to 10 kVA reactive load

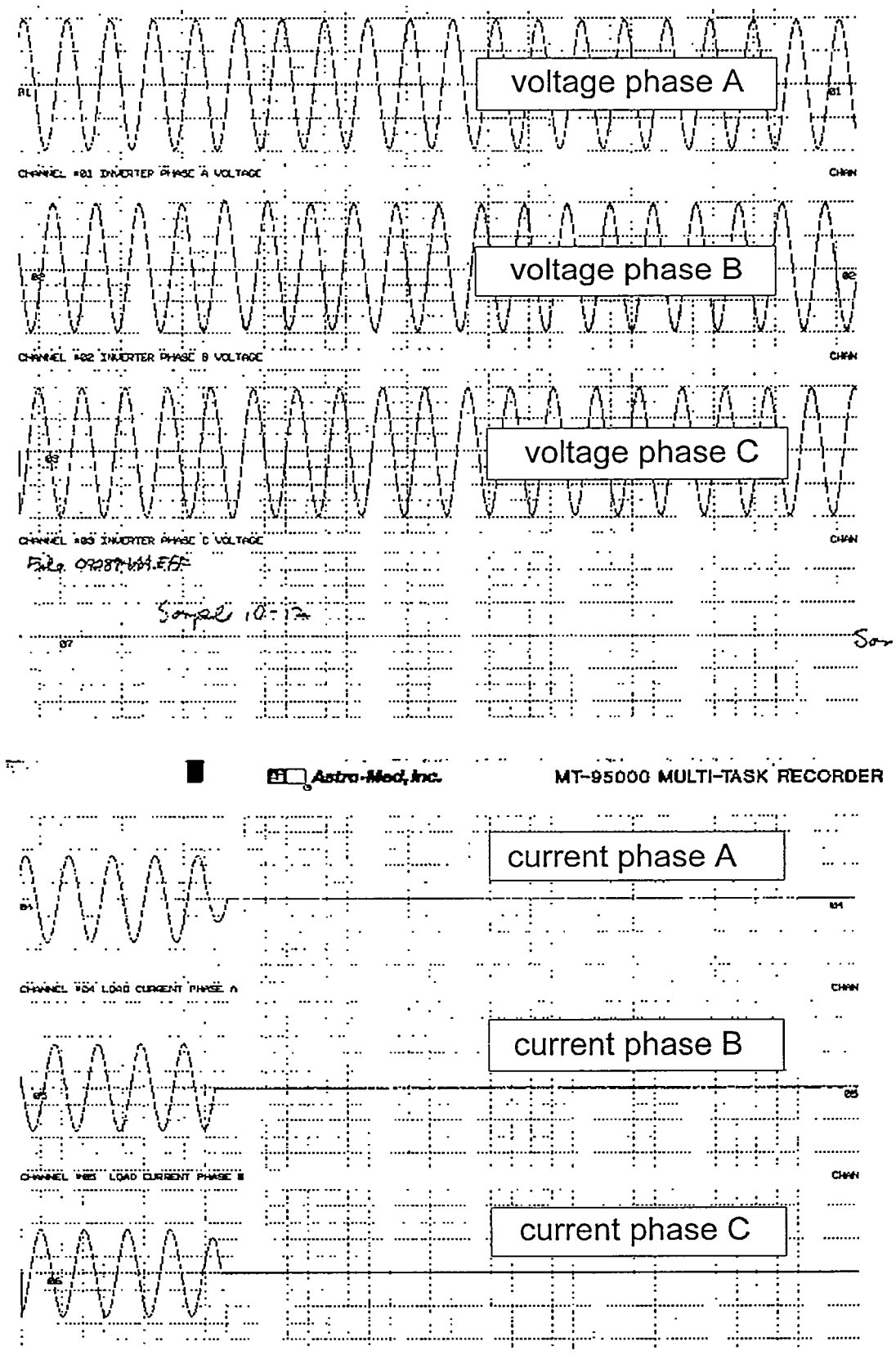

Chart 4: Transfer from 10 kVA reactive load to no load

Comparison to diesel. It is interesting to compare the inverter performance to that of the SNL diesel engine. The comparison is made for data that were acquired after the current limitation modification. That comparison is made in Table 4. The 75 kW diesel did perform a little better than the inverter in voltage regulation; however, the inverter is well within Abacus specifications (± 2%).

Table 4: A comparison of diesel and inverter performance during a 10 KVA step of load impedance

(maximum observed deviations)

source	voltage regulation	frequency regulation
inverter	1.4%	Δf = 0 Hz
diesel	.3%	Δf = 0 Hz

3.2.2 Efficiency

The efficiencies of interest are those of the inverter (both directions) and the battery. The MPT was evaluated separately.

3.2.2.1 Inverter Efficiency

This test evaluated the efficiency of converting dc power to ac power. The inverter efficiency was evaluated using the following load profiles.

1) A stepped resistive load from no-load to full load (10 steps). The loads were balanced on all three phases. The measurements were repeated for two values of dc input voltage: V_{min} and V_{nom}.
   with V_{nom} = 192 volts
   with V_{min} = 180 volts

   The output is two curves (one for each battery level) of efficiency versus load (see Figures 1 and 2). An accompanying curve of battery voltage versus load level is also presented for each of the efficiency plots.

2) Reactive loads, a 10 kW resistive load on phases B & C and a 10 kVA load with a power factor of .5 ,.6,.7, .8, & .9 inductive on phase A, all three phases fully loaded. The output is a curve of efficiency versus PF for phase A (see Figure 3). An accompanying curve of battery voltage versus pf is presented.

3) A nonlinear load composed of
   1,2,3,& 4 kW nonlinear and a 870 W resistive load on phase A
   870 W resistive load on phase B
   870 W resistive load on phase C

   The nonlinear loads were comprised of parallel full-wave rectifier bridges with discharge resistors across the dc output capacitors. The efficiency is shown in Figure 4.

4) Peak load efficiency. This measurement was recorded during the Load Handling Capability Test .
   12 kW resistive load

12 kVA load with power factor of .5 inductive
17 kW resistive load.

The efficiency is shown in table 5.

Test Configuration.

PV power = disconnected

loads = as specified

diesel = off, inverter forced on.

battery SOC = variable

Data:

The efficiency for resistive loads peaks at 91% for a system load of 25 kW (Figure 1). It should be kept in mind that this is the maximum efficiency when sizing loads. The battery voltage is plotted because parameters such as efficiency could change with changes in battery voltage. It turns out, however, that the efficiency did not vary with battery voltage (Figure 2). As expected, if volt-ampere values were compared to watt values reactive loads resulted in lower efficiencies (Figure 3). The efficiency also drops significantly for nonlinear loads. For example, with a current distortion of 65%, the efficiency is only 60% at 4200 volt-amperes. Finally, Table 5 displays the efficiency for the peak operating points of 12 kVA.

Table 5: Efficiency of Peak Loads

Load	Efficiency
12 kW resistive load	0.9
12 kVA load with power factor of .51 inductive	0.84

The inverter was successfully loaded to 17 KVA/phase for about five minutes. At that point the 70 ampere circuit breaker tripped, ending the test. The 70 ampere rating of the breaker was exceeded. The four efficiency plots are shown in Figures 1 through 4.

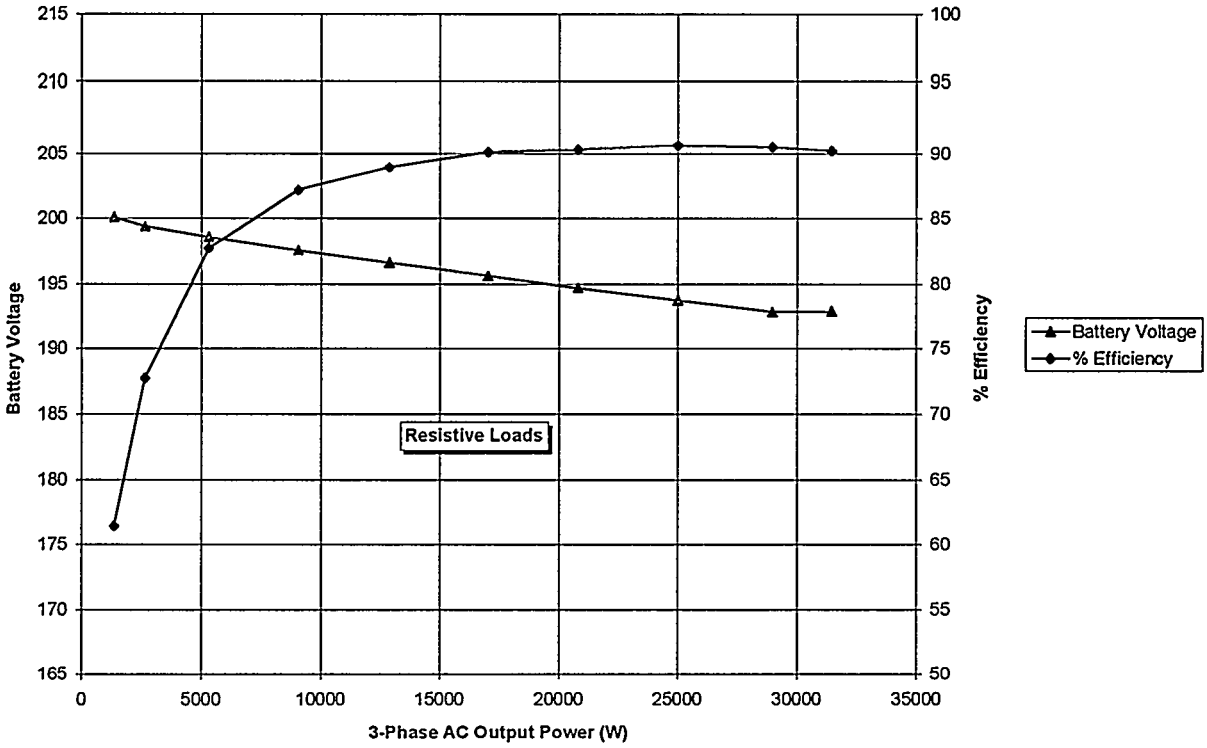

Figure 1: Efficiency versus power with nominal battery voltage

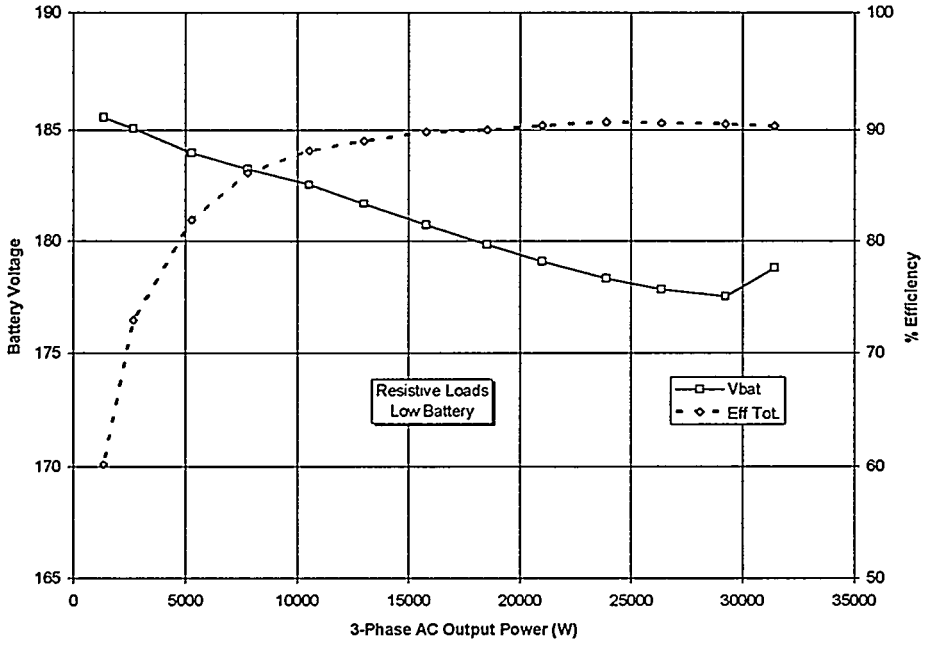

Figure 2: Efficiency versus power with low battery voltage

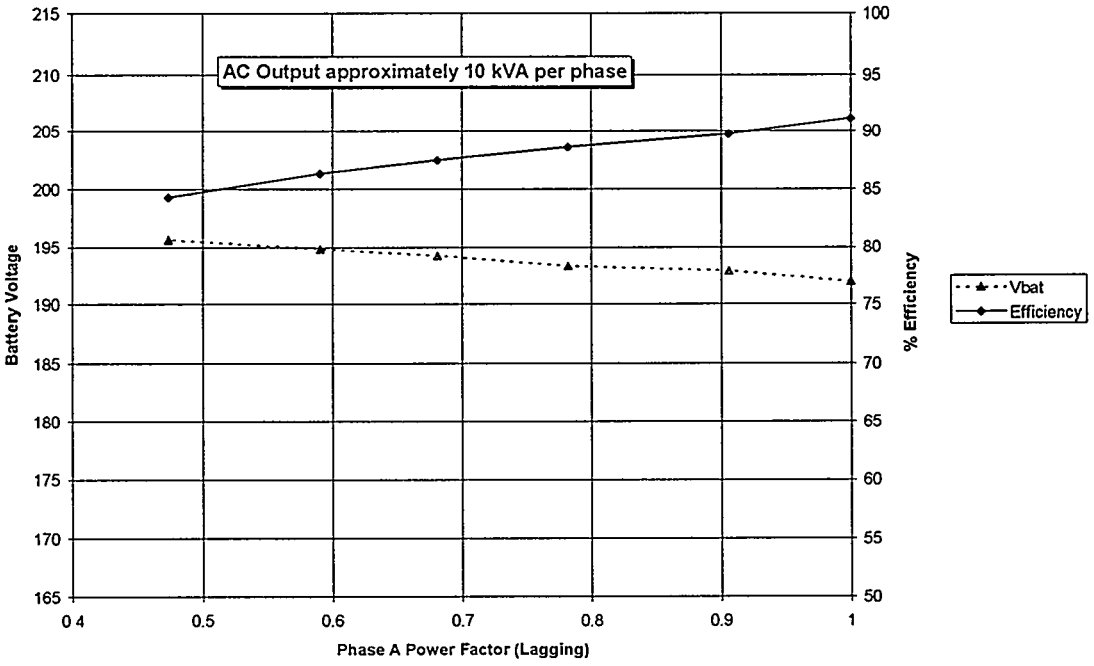

Figure 3: Efficiency versus power factor for an R-L load

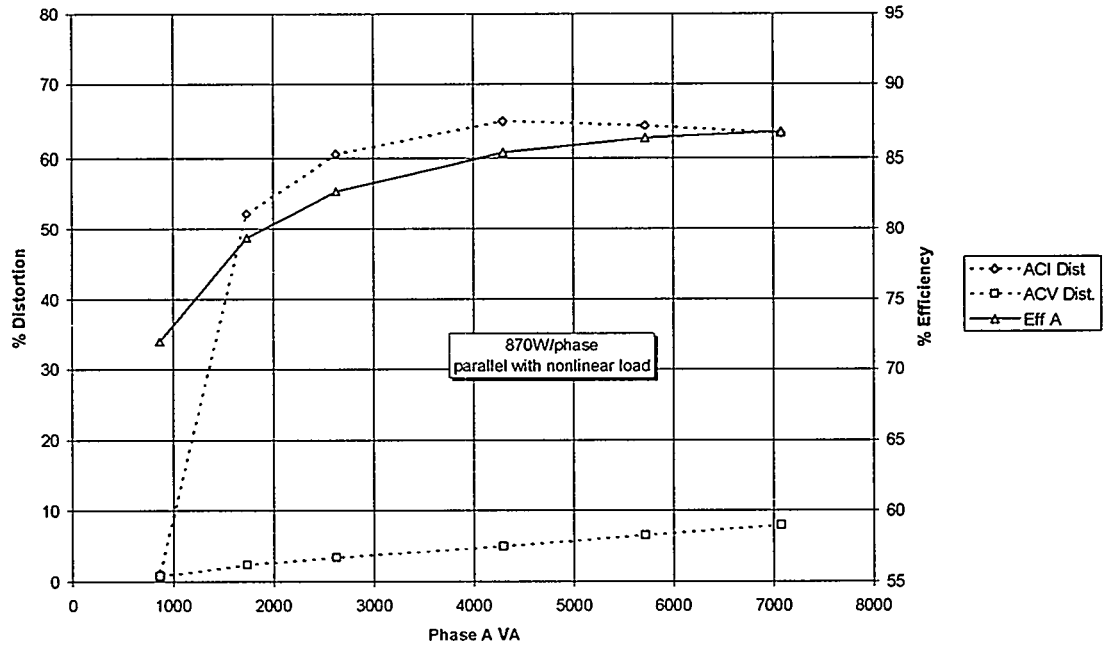

Figure 4: Phase A efficiency and distortion versus volt-amps

3.2.2.2 Charger Efficiency/Charge Rate

Because the battery charger efficiency of the Abacus bimode® inverter is affected by the battery voltage, the power into the inverter (from the "diesel") and out of the inverter (to the batteries) was monitored for a complete charging cycle, 175 Vdc to 222 Vdc.

The maximum inverter charge current and the maximum dc current were recorded.

Test Configuration.

PV power = disconnected

loads = disconnected

diesel = grid voltage substituted

loads = disconnected

battery SOC = discharged to 180 Vdc (loaded with 2 kW) for start of test

Data

The data are displayed in Figure 5. The efficiency of the battery charger was >89% during the time that all three inverters were charging. During this time period, the charging current started at 118 amperes and decreased slightly as the bus voltage increased. When the dc bus reached 221 volts, phase B discontinued charging. The bus voltage immediately dropped to approximately 217 volts and then climbed to approximately 221.5 volts dc. At this point, phase A stopped charging. Phase C continued to charge with approximately 38 amperes until the bus finally reached 222 volts dc. At that point phase C changed from a steady current source to a pulsating current source.

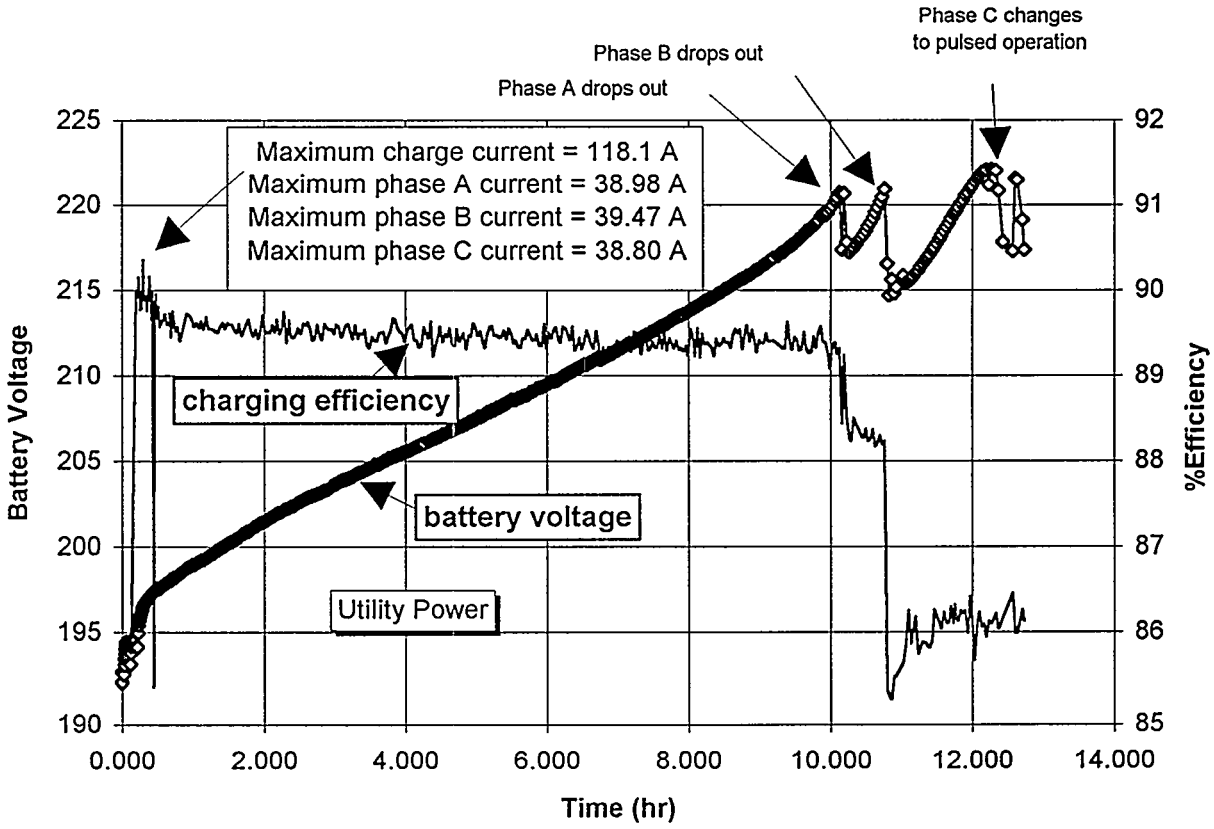

Figure 5: Battery voltage and charger efficiency versus time

3.2.3 Load Handling Capability

A discussion of how the maximum power capability of the inverter was evaluated appears below.

3.2.3.1 Evaluation of Rated Capacity

Abacus specifies a maximum of 10 kVA/phase; however, an excess power threshold (set in the firmware) of 8 kVA will start the diesel unless the diesel is disabled. Thus, for the purpose of this test, the diesel was disabled. During this test the ambient temperature was monitored. A temperature sensor was placed on the switching semiconductor heat sink to determine its maximum operating temperature. The test was conducted with the inverter fully loaded for a minimum of two hours. When the inverter heat sink temperature was stabilized with full load, and when the total time under full load was at least two hours, the test was concluded.

Similar tests were attempted for the following conditions:

1) 12 kVA load for 30 minutes
   12 kW resistive load
   12 kVA load with power factor of 0.5 inductive
2) 17 kVA load for 10 minutes
   17 kW resistive load.

Test Configuration.

array = disconnected

loads = variable

diesel = off (inverter forced on)

battery SOC = nominal

Data

The inverter was successfully loaded to 17 KVA/phase for about five minutes (see Table 6). At that time, the 70 ampere dc inverter circuit breaker tripped, preventing the ten minute operation. The circuit breaker rating was exceeded by the inverter. Since, for a constant output power, the dc current increases as the dc voltage decrease the precise value of this breaker that would supply 17 kW for ten minutes depends on the battery SOC. The inverter did handle 12 kW for 30 minutes and a load of 11 kW for one hour. In addition, it handled 10 kW for two hours and 12 KVA with a power factor of 0.5 for 30 minutes. Except for the limitation of the 70 ampere breaker, the inverter met or exceeded specifications.

Table 6: Rated Capacity Evaluation Summary

kVA/phase	power factor	minutes operated
10	1.0	>120
11	1.0	>60
12	.5	>30
12	1.0	>30*
17	1.0	5**

* test terminated due to exceeding 70 A dc breaker rating
** 70 A dc breaker tripped

3.2.3.2 Nonlinear Loading

Nonlinear current results whenever the circuit impedance varies as a function of time. It may vary from infinity to less than an ohm over the 60 Hz period. One adverse effect of the nonlinear current is that the normal sinusoidal voltage waveform is distorted by this type of current. This distortion may result in improper operation of some sensitive electronic equipment.

The nonlinear loads were provided by up to eight full wave bridges, connected in parallel with each other and with a variable pure resistance. Each bridge provided a load of 1200 watts. The data that follows show results for the nonlinear load with and without a parallel, pure resistive load. The recorded parameter is distortion. Fourier analysis of the data shows that the TD is equal to the measured value of distortion. Three items were of concern:

- nonlinear power levels that exceed 5% TD,
- nonlinear current levels that the 10 KVA phase A the bimode® can supply, and
- comparison to the SNL 75 KVA diesel generator?

Test Configuration.

PV power = on

loads = nonlinear, as required to get up to 76% current distortion for a 10 kVA load on phase A. A resistive load may be applied in parallel with the nonlinear load. The resistive load is applied equally to all three phases.

diesel = off (inverter forced on)

battery SOC ≅ nominal

Data

The voltage TD is related to both the peak value of the nonlinear current and the current TD. Also, the TD is increased when the inverter current limits at 70 amperes. The current limiting results in a reduction of the peak output voltage and an increase in the voltage distortion. In the data that follows, the nonlinear load is sometimes the only load and is sometimes paralleled with a pure resistive load. The resistive load draws current throughout the period of the waveform and is seen as a ramp under the nonlinear spike (Figure 7). Resistance in parallel with a nonlinear load decreases the I_{TD}. The phase A voltage and current TD are listed in Table 7. Prior to acquiring the nonlinear load data, the inverter was fully loaded with 10.35 kW of pure resistance; the current distortion was 3.9%. The voltage and current TD versus nonlinear load are shown in Figures 9 and 10. Although the specifications are for THD, TD is the measured parameter. These numbers are frequently identical; however, THD is never greater than TD.

Table 7: Result of Nonlinear Loading

case	voltage source	nonlinear load (kW) (approx values)	resistive load (kW)	% TD - voltage	% TD - current	power to load (kW)	volt-amps to load (kVA)
1	inverter	0	10.35	3.9	3.9	10.35	10.35
2	inverter	0	.87	1.2	1.2	.87	.87
3	inverter	1.17	.87	3.5	69	2.08	2.63
4	inverter	4.8	.87	7.9	63	5.37	7.08
5	inverter	2.34	0	5.23	75.9	2.34	3.68
6	inverter	4.5	0	8.25	70.2	4.5	6.5
7	inverter	8.14	.44	13.46	49	9.25	10.99
8	inverter	2.34	.44	5.1	70.5	2.80	4.0
9	grid	2.34	.44	1.6	77	2.6	4.16
10	generator	2.34	.44	5.08	71.3	2.82	4.05
11	inverter	2.34	3.70	4.68	40.7	6.25	6.84
12	generator	2.34	3.70	4.87	42.2	6.2	6.8
13	grid	2.34	3.70	1.57	47.7	5.9	6.74

The data from the table are explained below.

- Case 1: Baseline case. This case documents the distortion value of < 5% for a full power, resistive load.

- Case 2: Displays the waveforms for a pure resistive load that was placed in parallel with the nonlinear loads for cases 3 and 4 (see Figure 6).
- Case 3: Places a nonlinear load of 1.2 kW in parallel with 870 watts which results in a very high value for the I_{TD} (see Figure 7).
- Case 4: This rather high value of nonlinear load results in a I_{TD} of 63% and a V_{TD} 0f 7.9% (see Figure 8). Although the nonlinear load increased by a factor of four, the distortion decreased slightly. This condition results from the increased width of the current pulse; the pulse more closely resembles a sinusoid and thus the distortion is lower.
- Case 5: This purely nonlinear load draws 2.34 kW. Although the peak current is only 40 amperes, the high I_{TD} results in a voltage TD of 5.23%.
- Case 6: The purely nonlinear load of 4.5 kW has resulted in a V_{TD} of 8.12%. The inverter is operating perfectly, however, and could easily power most loads. Note that volt amps are much larger than watts.
- Case 7: At 70 amps of current, the inverter limits the current. This results in a flat top on the nonlinear current. The V_{TD} is 13.5%, however, the inverter is still able to power the nonlinear load. Because the inverter cannot supply the peak current that a utility could, it simply makes the current spike wider and thus supplies the same amount of energy to the nonlinear load.
- Case 8: The addition of 440 watts of resistive load in parallel with the 2.34 kW of nonlinear load decreases the voltage TD to 5%. The peak current, however, is about 42 amperes. Note that the current TD has been reduced to 70.5%.
- Case 9. Utility powers the same load as the inverter in Case 8.
- Case 10. Diesel powers the same load as the inverter in Case 8. Note that the diesel had a TD comparable to the inverter for the same load.

  Note: The following three plots have the same load impedance and different sources.
- Case 11. Although this case has the same nonlinear load as that depicted in Case 5, the addition of the resistive load has reduced the I_{TD} from 75.9% to 40.7% and consequently the total V_{TD} has been reduced from 5.19% to 4.68%.
- Case 12. Note that the generator has a slightly higher V_{TD} than the inverter. The I_{TD} also increases slightly, but this is due to the difference in the source; the load is unchanged from Case 10.

  Case 13. Again, the grid has the lowest V_{TD}.

Returning to the three questions posed earlier,

1. At what nonlinear power levels did the voltage TD exceed 5%? The question is too simple. The answer is that it depends on the load that parallels the nonlinear load and on the nonlinear current shape. A modest nonlinear load with a small parallel resistive load (case 4) can result in $V_{TD} > 5\%$, while a larger nonlinear load (case 7) can result in $V_{TD} < 5\%$. **Nonlinear load and V_{TD} do not have a simple relationship.**
2. How much nonlinear current can the 10 KVA phase A of the bimode® supply? The inverter successfully supplied approximately 8.1 kW of nonlinear load. At this point

the peak value of nonlinear current was limited by the inverter. The addition of more nonlinear current resulted in a broadened current pulse, which actually decreased current distortion.

3. How does the inverter compare to the SNL 75 KVA diesel generator? The inverter V_{TD} was no worse than that of the diesel.

Conclusions: When powering nonlinear loads, the most important aspect is that the power source be able to supply the energy needs of the load; the Abacus inverter met the load requirement. Requiring the THD to be less than 5% for all loads in hybrid systems is an arbitrary and frequently unnecessary restriction on hybrid power sources. However, because it is difficult to ascertain a given THD that is acceptable to a particular load, it is important to make some restriction on THD for village and SERDP inverters. **Therefore it is recommenced that, for hybrid photovoltaic systems, the THD be specified as <5% for all *linear* loads.**

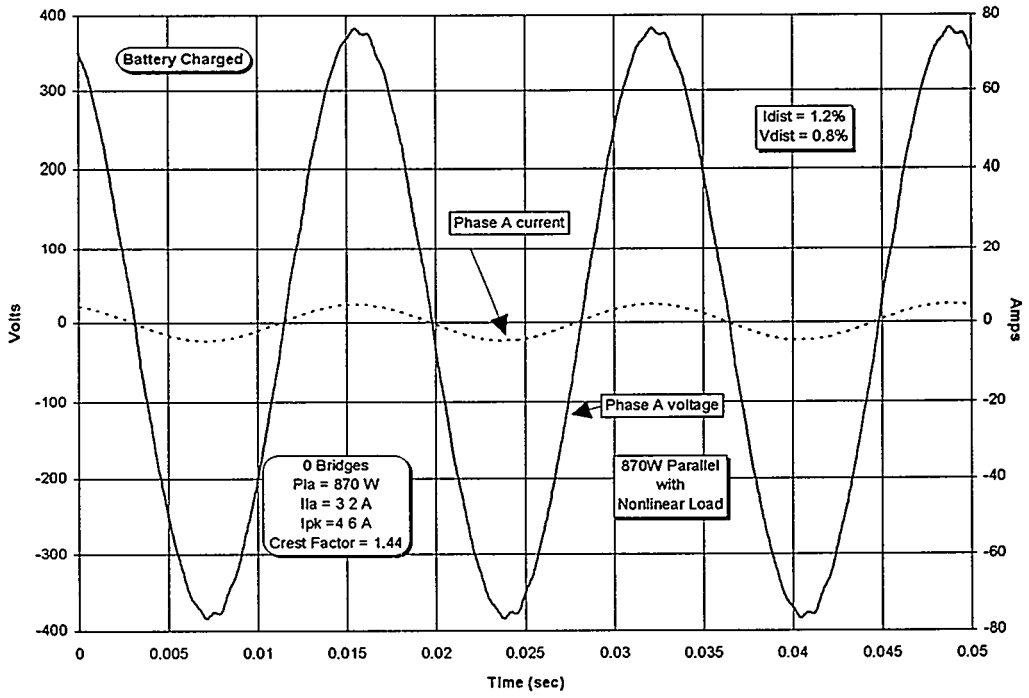

Figure 6: Inverter output with 870 watts/phase resistive load

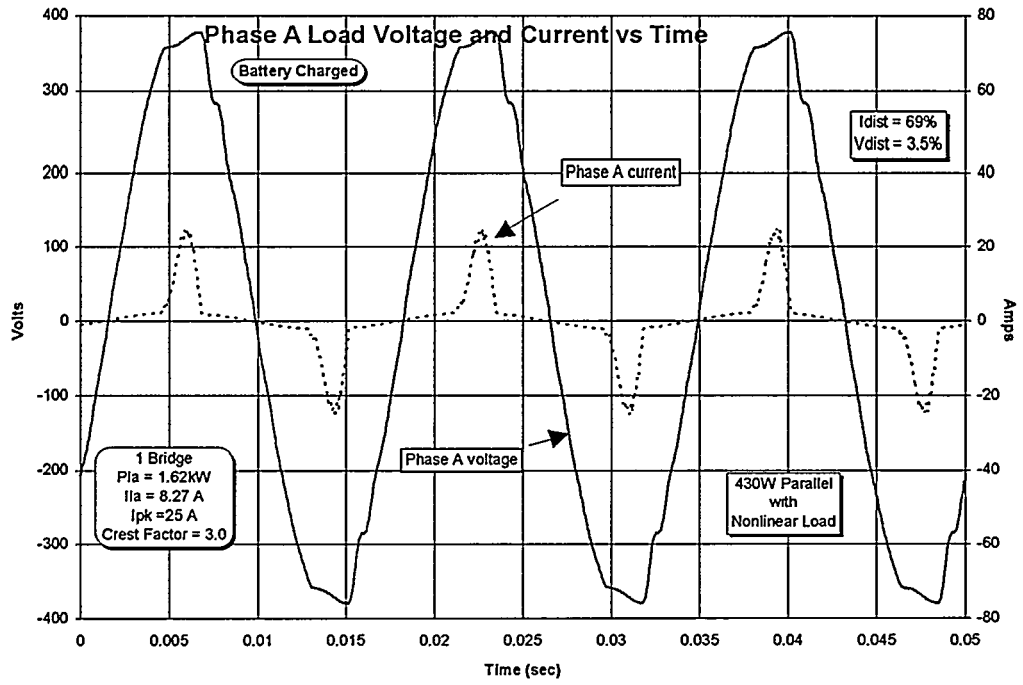

Figure 7: Inverter output with 870 watts/phase resistive load in parallel with 1.2 kW nonlinear load

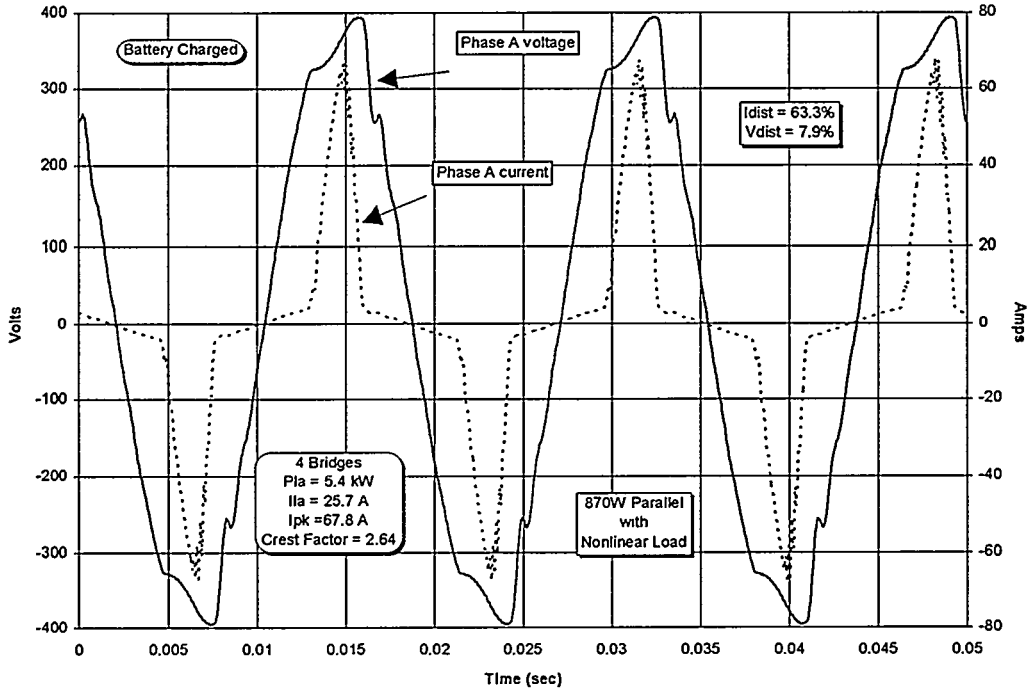

Figure 8: Inverter output with 870 watts/phase in parallel with 4.8 kW of nonlinear load

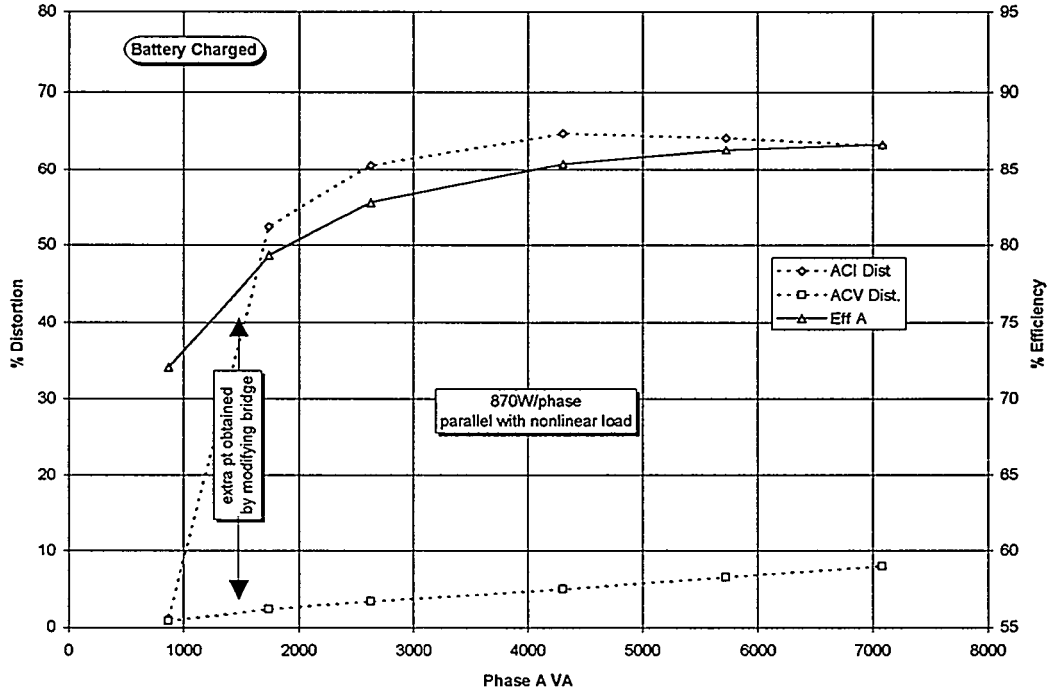

Figure 9: Phase A distortion and efficiency for a fixed resistive load of 870 watts and a variable nonlinear load

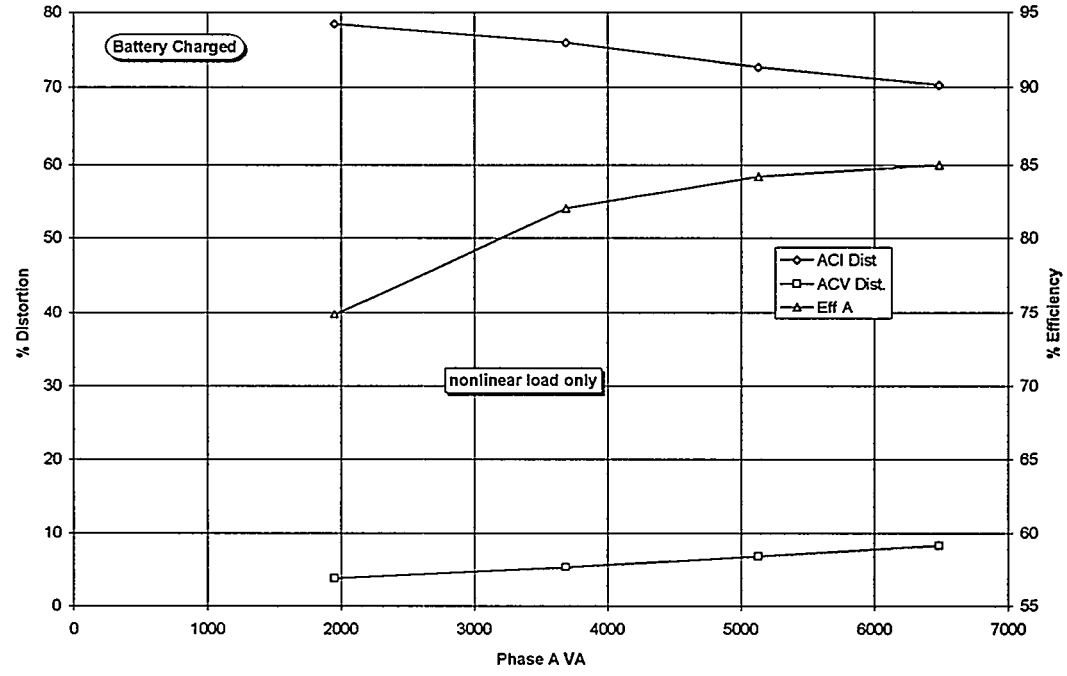

Figure 10: Phase A distortion and efficiency for a zero resistive load and a variable nonlinear load

3.2.3.3 Surge Power/Transient Loading

Surge power is not specified in the Abacus specification; however, each phase was designed to withstand a 22 kW load for 3 seconds. This value was our target surge current. Built-in current limiting was expected to prevent the surge current from exceeding 70 amps. A transient load was provided by a three-phase, 15 ton Trane air conditioner, Model RAUD-404-E. Under steady-state conditions, the air conditioner provided a 4.5 kW/phase load. The frequency stability is specified as 60 ±.5 Hz for all required load conditions.

Test Configuration.

PV power = none

loads = three phase air conditioner.

diesel = off (inverter forced on)

battery SOC = nominal.

Data

The air conditioner was started using three different sources of ac power; the local utility line, the 75 kW diesel, and the Abacus inverter. The air conditioner voltage and current for each source are displayed in Figures 11, 12, 13, 14, and 15. In Figure 11, it was observed that the local line voltage was not distorted by the air conditioner startup. In Figure 12, single occurrence distortion is observed on the diesel output. Note that the utility and the generator are at steady-state by the fourth peak. The distortion of the inverter voltage is shown in Figures 13,14, & 15 for phases A, B ,and C respectively. The distortion was related to the phase angle at the time the inverter was turned on. The worst case is shown in Figure 13. The peak current in the first half cycle is 80 amperes for an instantaneous power of 22.1 kW/phase. The inverter does current limit this value of current during the first half cycle. Current limiting stops on the decreasing first half cycle of current and the inverter immediately corrects the voltage. This results in a voltage transient and an offset of the dc component of the ac output. By the second half cycle, the current is less than 70 amperes. The current is essentially at its steady-state value by the third cycle after the motor was energized. Thus the inverter compares very well in the category of motor start time. The inverter feedback loop is responsible for the second transient in Figure 13. This signal corrects for the dc offset and it can be seen that the occurrence of the second ac voltage transient is coincident with a shift in the dc component of the ac signal. The transients are smaller on phase B (Figure 14) and barely noticeable on phase C (Figure 15). The effects of a single transient are difficult to assess; however, the transient distortion resulting from the air conditioner does not appear to be significantly worse for the inverter than for the diesel. The inverter does give additional zero crossings of the 60 Hz voltage output.

It is interesting to observe the inverter current limiting engage. To observe this, a fixed resistive load of 4.8 kW was placed in parallel with the motor. The motor was energized after the resistive load. These data are shown in Figure 16. The first half cycle shows a current of 25 amps peak being drawn by the resistive load. At a time of .01 seconds, the air conditioner motor is placed in parallel with the resistive load. Current limiting was observed on the first negative half cycle. When the same load is energized from the utility, the motor drew in excess of 100 amperes. Thus, unlike the situation shown in Figure 13, where the surge current was reaching only 80 amperes, the current

limiting was implemented immediately when this large excess current was demanded. The inverter acted very quickly to protect itself.

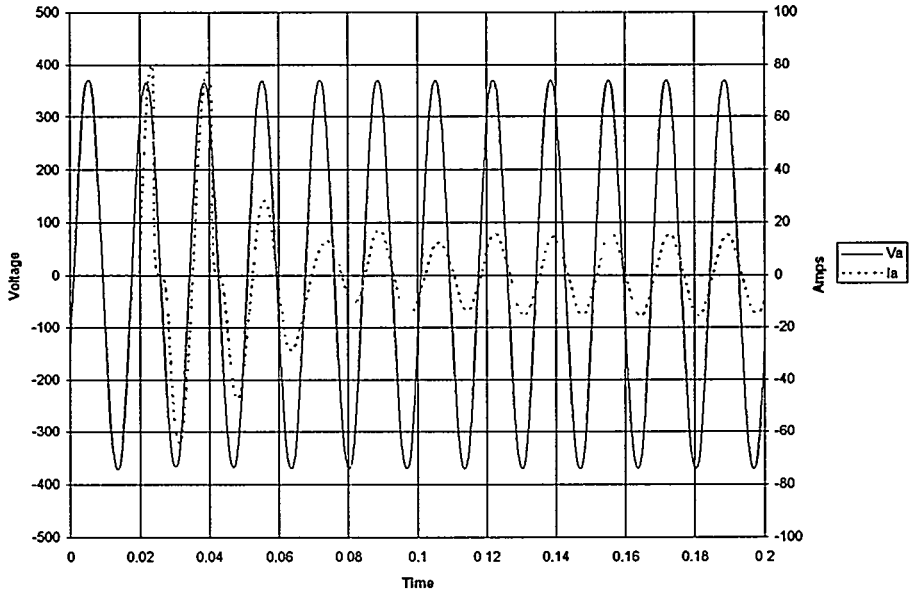

Figure 11: Air conditioner motor startup on utility

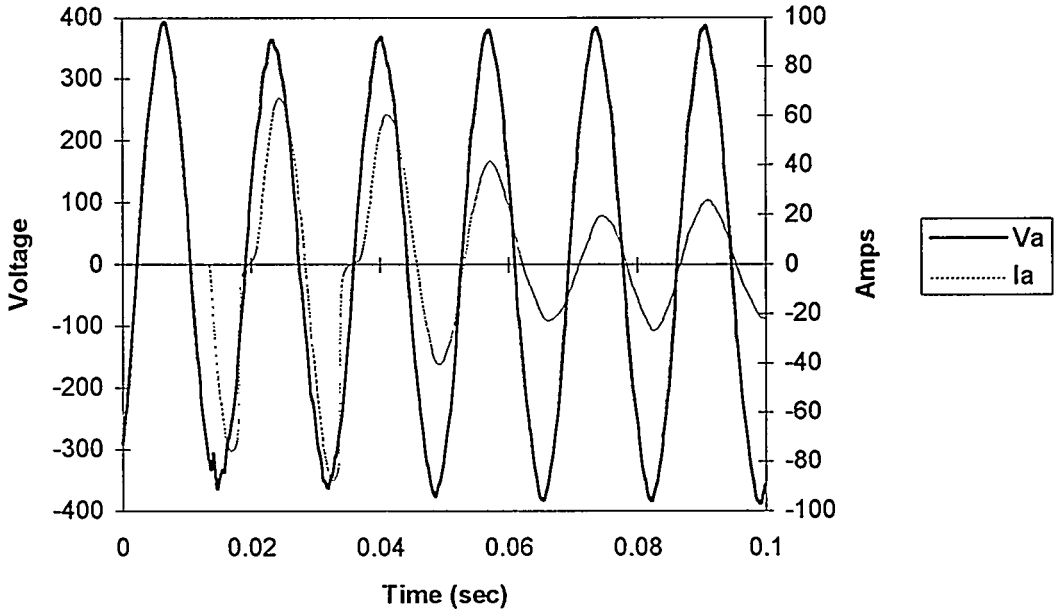

Figure 12: Air conditioner motor startup on generator

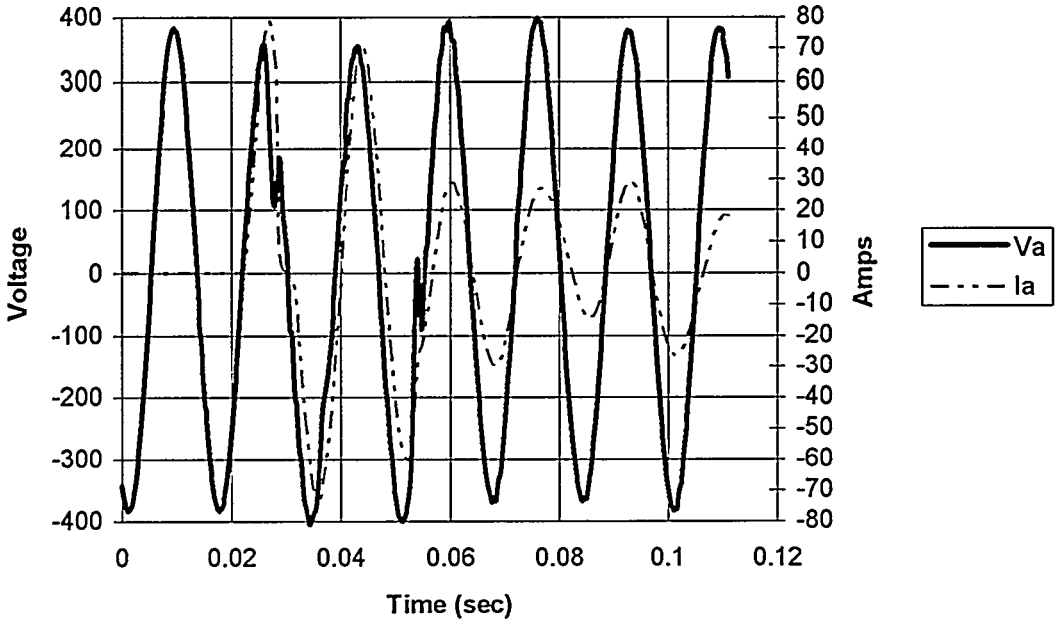

Figure 13: Air conditioner motor startup on inverter (phase A)

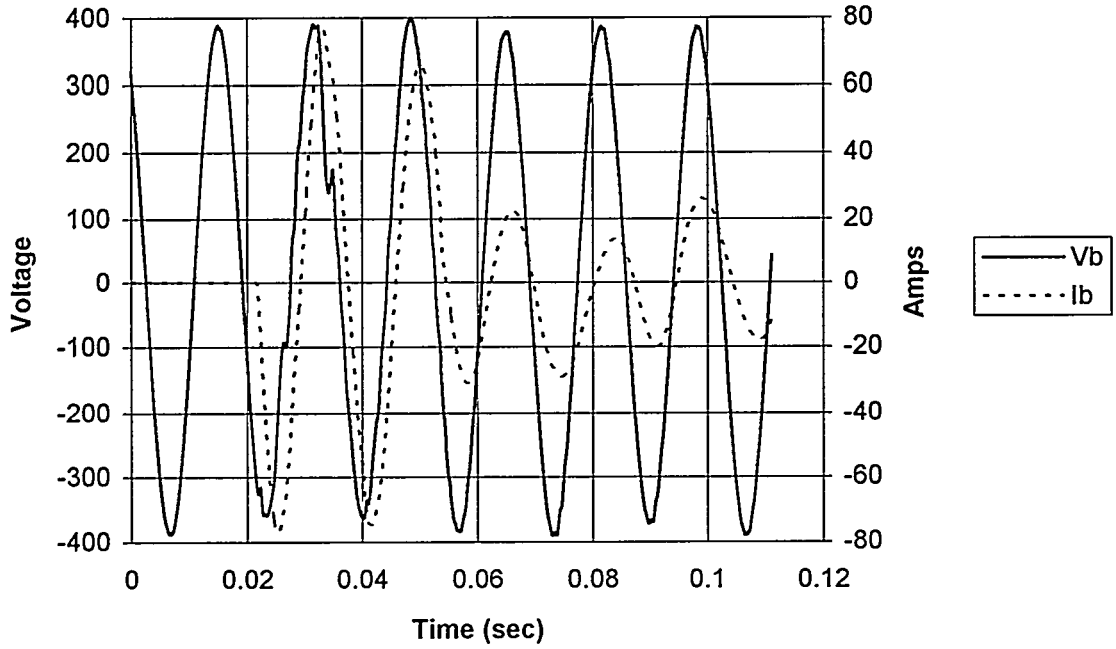

Figure 14: Air conditioner motor startup on inverter (phase B)

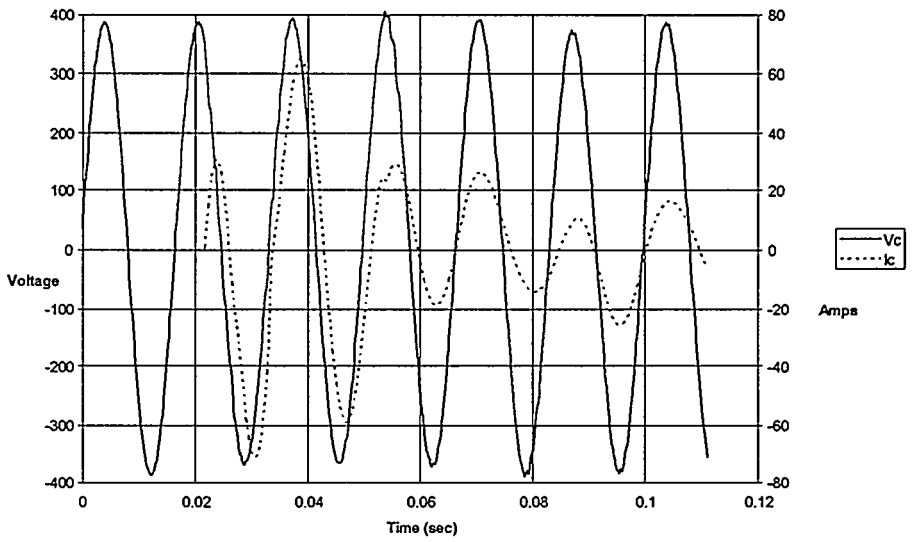

Figure 15: Air conditioner motor startup on inverter (phase C)

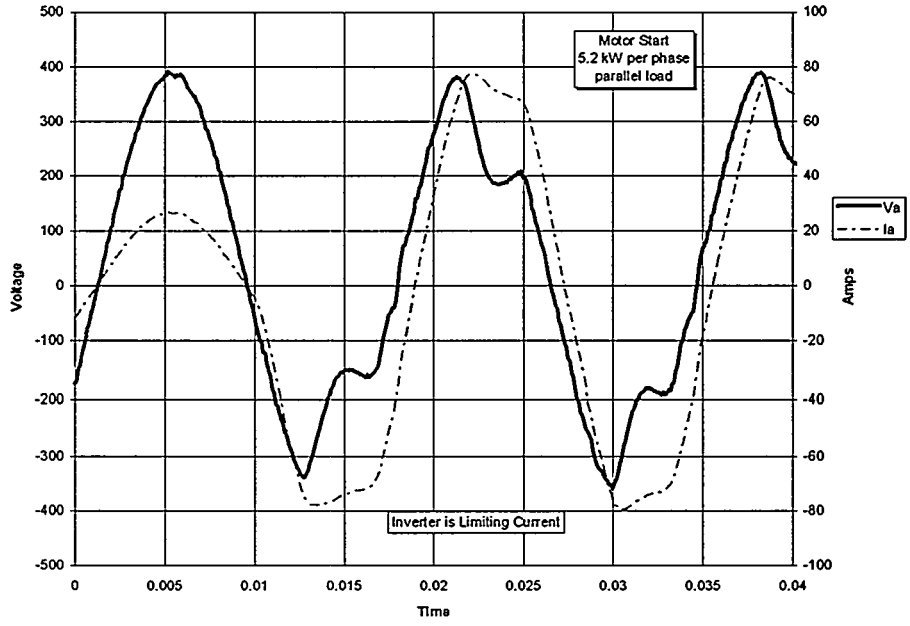

Figure 16: Air conditioner startup with current limiting demonstrated

3.2.4 Inverter Interface Issues

3.2.4.1 Input (dc Interface Issues)

3.2.4.1.1 Evaluation of Input Voltage Range

The inverter normally operates within the dc voltage range of $V_{min} < V_{dc} < V_{max}$. V_{min} is determined by the generator start voltage, 175 volts. Measurements were made for dc input voltages of V_{max}, V_{min}, and $V_{disconnect}$. The expected battery float voltage was 216 volts dc. V_{max} is determined by the battery voltage under load, using a fully charged battery. The inverter is specified to turn off if the battery voltage reaches $V_{disconnect}$ (168 Vdc). The inverter was loaded with 2.5 kW/phase during this test.

Test Configuration.

PV power = disconnected

loads = 2.5 kW/phase.

diesel = off (inverter forced on)

initial battery SOC = fully charged

Data

The test specific measurements included the battery voltage, and the generator on/off commands.

During the battery cycle, the following events occurred:

- While supplying a constant resistive load of 2.5 kW/phase, the generator finished charging the battery. The battery was charged to 221 volts dc.
- When the inverter stopped charging the battery, the battery bus voltage dropped immediately to 204 volts dc.
- The call for generator start (disabled for this test) occurred at 178 Vdc.
- Since the generator was not available, the inverter terminated battery discharge at 168 Vdc.

These events are summarized in Table 8.

Table 8: dc Input Voltages

Function	voltage
maximum operating voltage	204
generator turn-on voltage	178
battery disconnect voltage	168

3.2.4.1.2 Full Generator Utilization

If the actual load plus the desired battery charging rate exceeds the generator capacity, the inverter is supposed to fully load the generator without overloading it. This is accomplished by reducing the power flow through the charger when the load exceeds the sum of the desired battery charging power and the load power. The diesel power rating of 75 kW is preset in the inverter firmware. To verify this capability, the inverter was placed in the charge mode, and an increasing resistive load was placed in parallel

with the charger. The diesel load should equal the sum of the battery charging and the resistive loads placed on the inverter output.

Test Configuration.

PV power = disconnected

loads = initially 6 kW/phase, resistive

diesel = on

battery SOC ≈ 80%

Data

The load was steadily increased during the time interval from 9:38 until 9:53 a.m. (see Figure 17). The charging power was relatively constant until the load reached 40 kW. At that point, the charging current dropped until the load reached 70 kW (diesel power equal to 74 kW). When the load was reduced, the charging current returned to its previous level. Note that, since the charging power (current) is inversely related to the battery voltage, the charging power for this nominally charged battery is less than the 25 kW maximum that the inverter is capable of drawing.

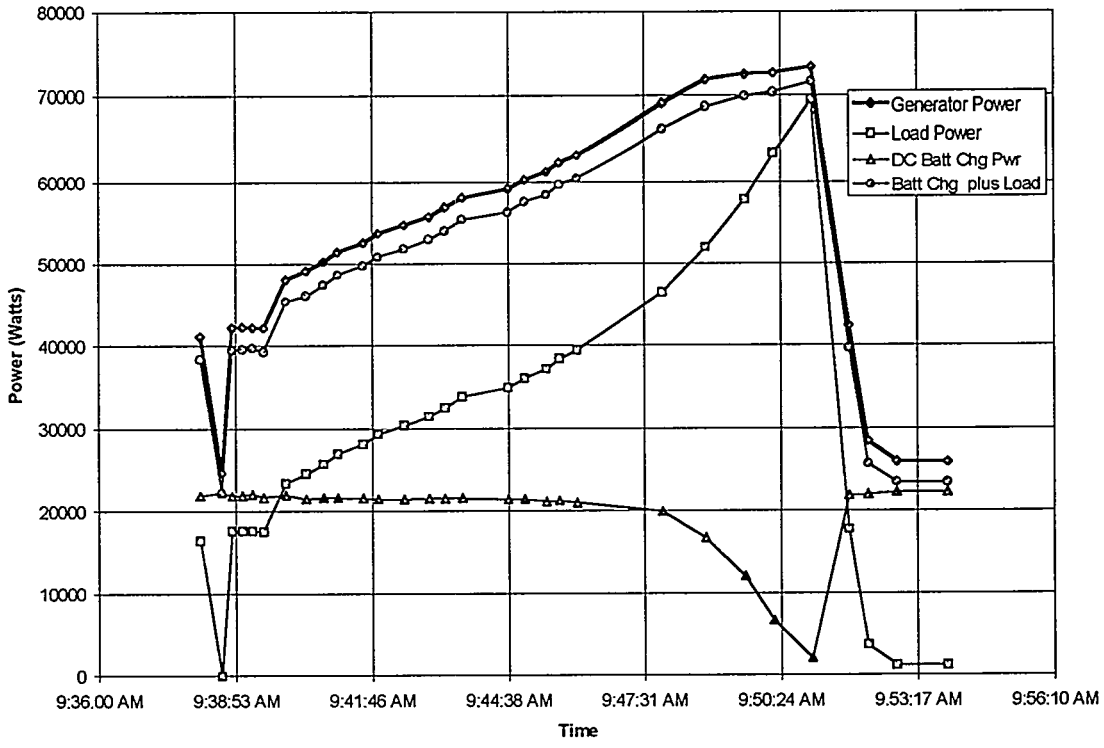

Figure 17: The effect of load on charge current

3.2.5 Radiated and Conducted Radio Frequency Emissions

Electromagnetic emanations fall into two categories: radiated and conducted. The Federal Communications Commission (FCC) regulations for electromagnetic radiation limits generally apply; however, the conducted emissions are required legally only when

connected to a commercial grid. Compliance with FCC Part 15 is a desirable goal for large hybrid systems and SNL therefore evaluates all inverters as if the regulation applied. In rare instances, MIL-STD-461C is required for military applications. Because that standard is so voluminous, these requirements are addressed only as needed and were not addressed in these tests.

Although FCC Part 15 applies only to grid-tied electronics, electrical emanations were examined to determine their compliance with FCC Title 47 of the Code of Federal Regulations, Part 15 "Radio Frequency Devices" Subpart J - "Computing Devices". These measurements are difficult to perform accurately; certification must be accomplished by an independent test laboratory.

The regulations are summarized in Table 9.

Table 9: Summary of FCC Regulations for Part 15

Transmission Mode	frequency	Class A	Class B
radiated	30 - 88 MHz	300 μV/m at 3 m	100 μV/m at 3 m
radiated	88 - 216 MHz	500 μV/m at 3 m	150 μV/m at 3 m
conducted	.45 - 1.5 MHz	1000 μV	250 μV
conducted	1.6 - 30 MHz	3000 μV	250 μV

3.2.5.1 Radiated Measurements

The frequency spectrum that FCC Part 15 addresses for radiated emissions is so high that no problems have been observed on any of the PV inverters that have been tested. There have been radiated emissions problems in the AM radio and TV spectrums. This area is not covered by FCC Part 15; however it was examined in the SNL tests.

Part 15 requires an "open, flat area" that shall be "void of buildings, electric lines, fences, trees, & etc.". Because SNL is not providing a "certification" of the hardware, and because the radiated inverter noise is low frequency (principally < 100 kHz) and will not reflect from surrounding objects significantly, the testing was conducted indoors. Background noise was surveyed prior to conducting the test. Background measurements that are 10 dB less than the acceptable levels, as specified in Table 9, would not interfere with this test. If background signals are too high, the test would be moved to a more isolated area or adjacent equipment would be turned off until the background is acceptable. EMI from the inverter should not interfere with equipment that is 2 meters away. EMI should be suppressed on both the ac and dc sides, as required.

Data

Observable radiated emissions did not exceed the allowable thresholds. There were many discrete frequencies where the spectrum was not observable, due to the high level of local RF emanations. Because the inverter noise, as observed with a near-field probe, are very broad band, it is believed that these local discrete radiators did not "hide" any discrete noise problems from the inverter. Thus the inverter appears to have passed the radiated RFI specification; however, this cannot be conclusively determined at this location.

3.2.5.2 Conducted Power-line Measurements.

This test was not performed due to test equipment malfunction.

3.2.6 Acoustic Emissions

The objective of this test was to determine the acoustic noise power in the audio spectrum that is generated by an operating power conditioning system.

The instrumentation used for these measurements was calibrated in dB spl with both A and C weighting and provided an AC output. SNL used the Bruel & Kjaer (B&K) Model 2230 Sound Level Meter with a Sound Level Calibrator. Instruments of this type include a calibrated microphone, signal conditioners, and a dB display in a single, hand-held unit.

The calibrator used with the B&K precision sound level meter must be within 3% of the stated frequency and ±1 dB at a level of 140 dB. The measurement has an intrinsic accuracy of about 1% but when the random background is considered, the errors combine calibrator accuracy and measurement accuracy to give 5% overall accuracy.

Data

The background noise (Figure 18) in the laboratory was measured with the B&K Precision integrating sound level meter located 0.5 meters from the front of the center cabinet of the three-phase bimode® inverter. The inverter is OFF, but the loads and all supporting equipment are running.

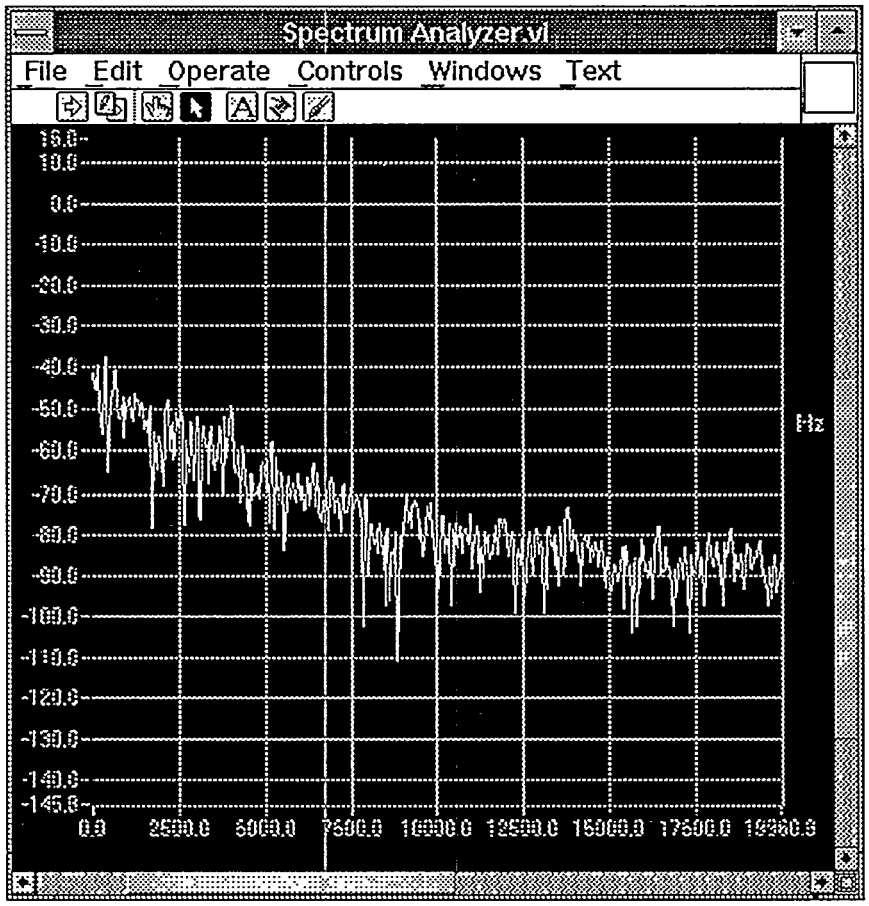

Figure 18: Background noise

The measurement was then taken with the inverter running with a 22 kW load and the B&K meter in same location. The noise peaks occur at about 5,700 Hz, and multiples of 5700 Hz (see Figure 19). The maximum dB reading was -40 dB at 5,700 Hz.

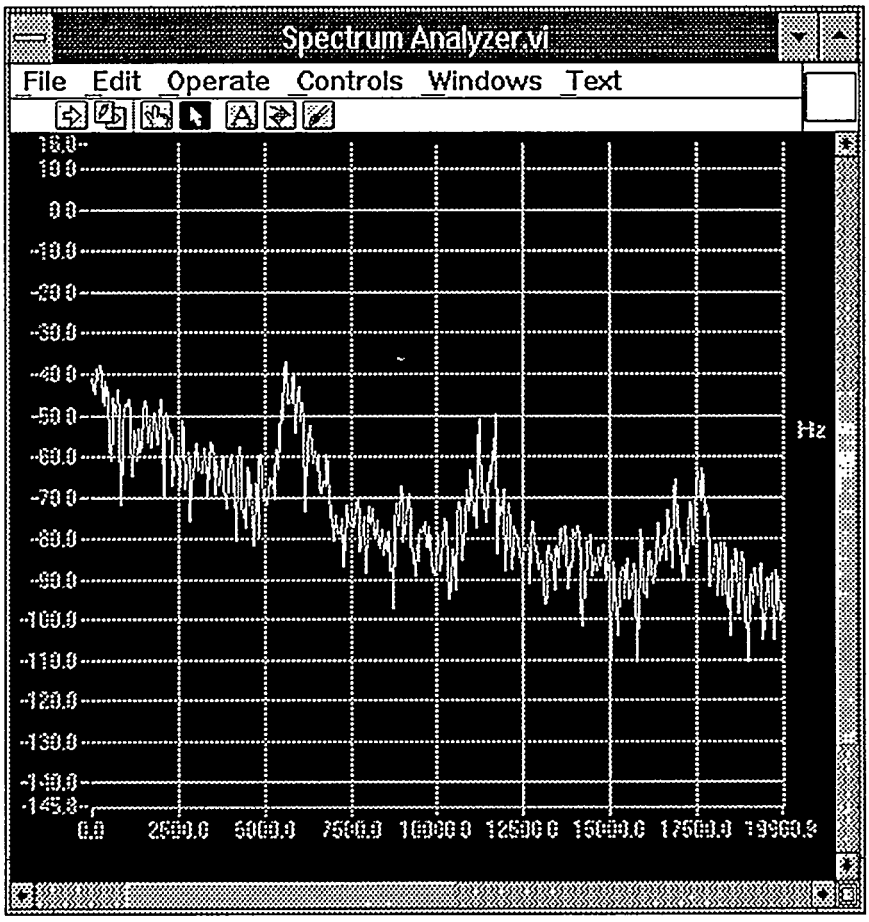

Figure 19: Inverter with 22 kW load

3.2.7 Maximum Power Tracking

The purpose of a maximum power tracker (MPT) is to increase the power transfer from the solar array to the MPT load (combination of battery and inverter). The MPT was evaluated while connected to crystalline silicon module strings. There were 470 modules available. They were configured in up to five strings of 72 modules per string. The parameters evaluated included efficiency, effectiveness, and operating limits. Because the solar irradiance is a key parameter for this test, sunny days were preferred.

The load on the MPT is also a key parameter. The load was the combined effect of the battery in parallel with the inverter. It was intended that battery voltage be relatively constant during some of the tests and thus present a fixed load to the array string/battery load. This condition can be achieved if the battery SOC is fixed. During some of the efficiency tests, the inverter load was kept approximately equal to the power input from the array strings/MPT. This kept the battery voltage fairly constant. Array output voltage was collected for each data point discussed below.

3.2.7.1 MPT Efficiency and Power Handling Capability.

The efficiency of a MPT is the ratio of the output power to the input power. For use with the MPT, the nominal array voltage, specified by Abacus, is 350 Vdc with maximum power tracking over the range of 280 V to 420 V. Measurements found that the typical Hughes module (the SNL array) has an open circuit voltage of about 6 volts and that it has peak power parameters of approximately 13.7 amps and 4.3 volts, or 59 watts. A string of 72 modules results in an expected maximum operating point of 310 volts for a power of 310 * 13.7 = 4,241 watts.

The MPT is rated at 25,000 watts when connected to a 240 volt battery string. In the SNL tests, the battery string was 192 Vdc nominal; this resulted in a derate of the MPT. The power output of the MPT is directly related to the output current. Thus for low battery SOC, when the battery voltage is lower, the MPT can handle less power. The rated power is 20 kW and refers to this low battery voltage situation. The tests below were conducted at nominal battery voltage and thus the expected MPT output power is > 20 kW.

Test Configuration.

PV = connected to MPT (configuration 5 strings)

loads ≈ variable from zero to 22 kW

diesel = off (inverter forced on)

battery SOC = nominal

Data:

The efficiency was evaluated for five strings of 72 modules. The inverter was loaded with 22 kW during this test. The MPT was evaluated by collecting efficiency data at one minute intervals. The maximum measured output power was 21,520 watts. The efficiency ranged from a low of 96.7% to a high of 99.4%. Figure 20 depicts the efficiency versus output power. The data have been sorted and replotted in Figure 21. The data show a correlation between these two parameters with efficiency decreasing as output power increases for the five string case.

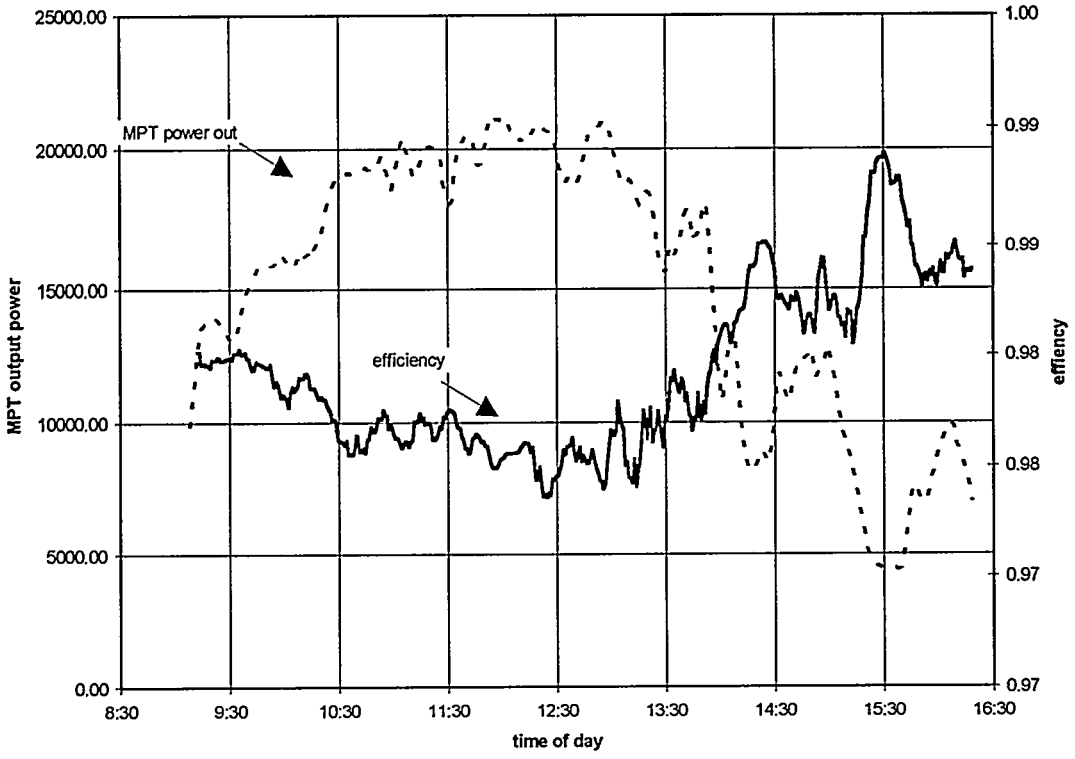

Figure 20: MPT efficiency and power versus time (five string case)

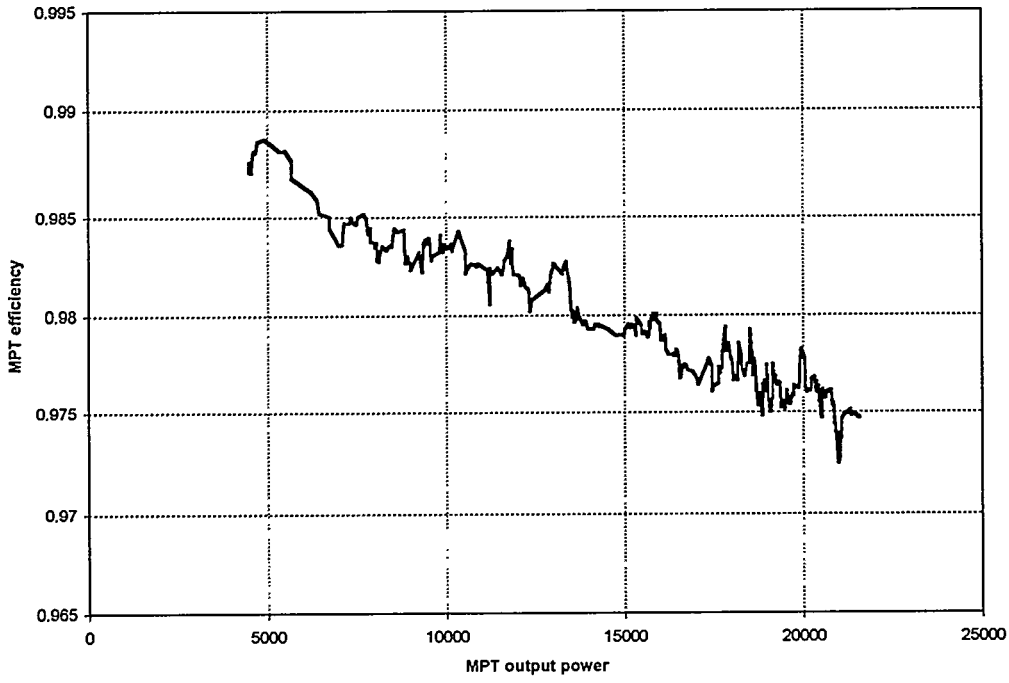

Figure 21: MPT efficiency versus output power (five string case)

3.2.7.2. Effect of MPT in Increasing Available Energy

It is expected that the MPT will increase the available energy. To provide some insight into this issue, a 51 module string was connected directly to the battery without going through the MPT. In addition, a single 72 module string was connected through the MPT to the battery. Because the data were collected simultaneously for these two strings of modules, they had the same insolation. During this test, the battery was loaded with a resistive load which drained the same amount of power as the MPT was producing. This kept the battery voltage very near its nominal value of 192 Vdc. The output power was then normalized to power per module, integrated and plotted.

The determination of the usefulness of an MPT is complex. Depending upon the module temperature and the I-V curve of a particular string. The 51 module string was configured to ensure adequate voltage to completely charge the batteries (see Figure 22); it was operating below its maximum power point at the nominal battery voltage of 192 Vdc. When the battery is discharged to a low voltage (down to 175 Vdc), the 51 module string is moved even further from its maximum power point. The further the battery voltage is from the maximum power point, the greater the benefit of the MPT to the system. A complete evaluation must be conducted over a complete range of battery voltages, modules temperatures, and values of insolation. The data provided in this report are interesting, but no conclusion is made regarding the usefulness of the MPT.

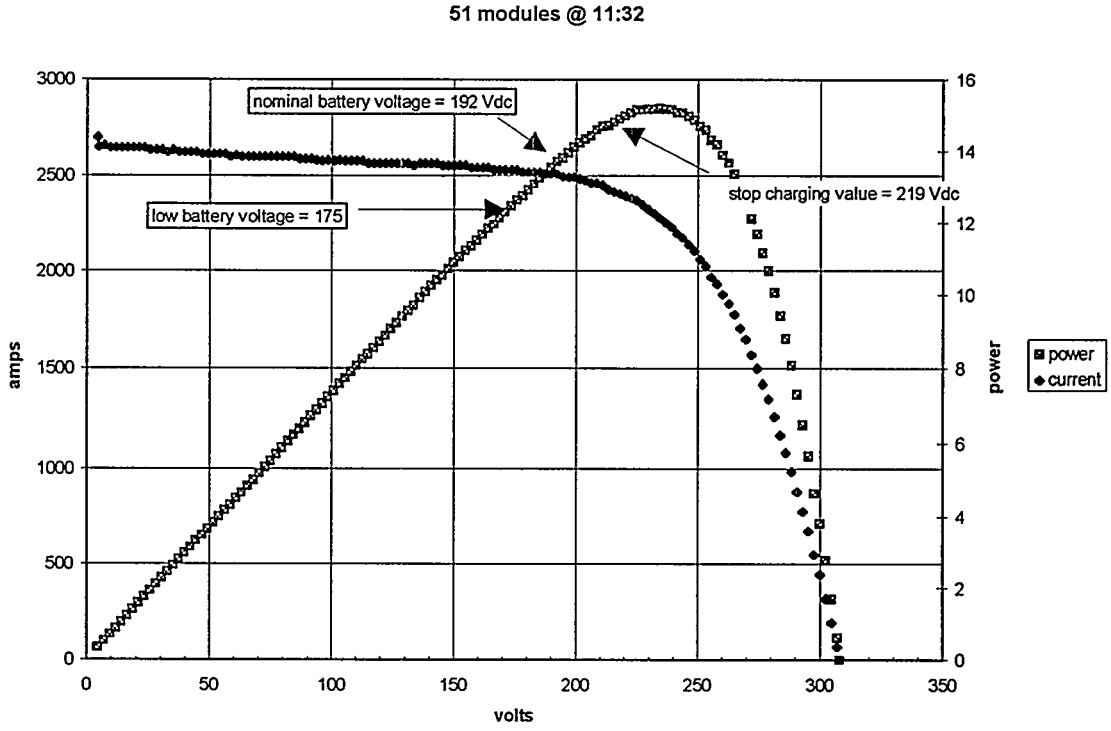

Figure 22: I-V and power curve for 51 module string

Data.

The data are shown in Figures 23, 24 and 25. It is observed that the normalized peak power for the direct case is 55.4 watts (figure 23), while the normalized peak power for

the MPT case is 59.55 watts. This is an increase in peak power of 7.5%. The energy increases from 349.5 watt-hours for the direct case to 356.1 watt-hours for the MPT case. This is an increase in energy of 2%. The output of the MPT is somewhat decreased because of the decreased efficiency from operating with only one string (see Figure 25). Thus, with 5 strings available, one could increase the MPT efficiency by approximately 1% during the high insolation portion of the day. This data adjustment results in a total energy increase of 3%.

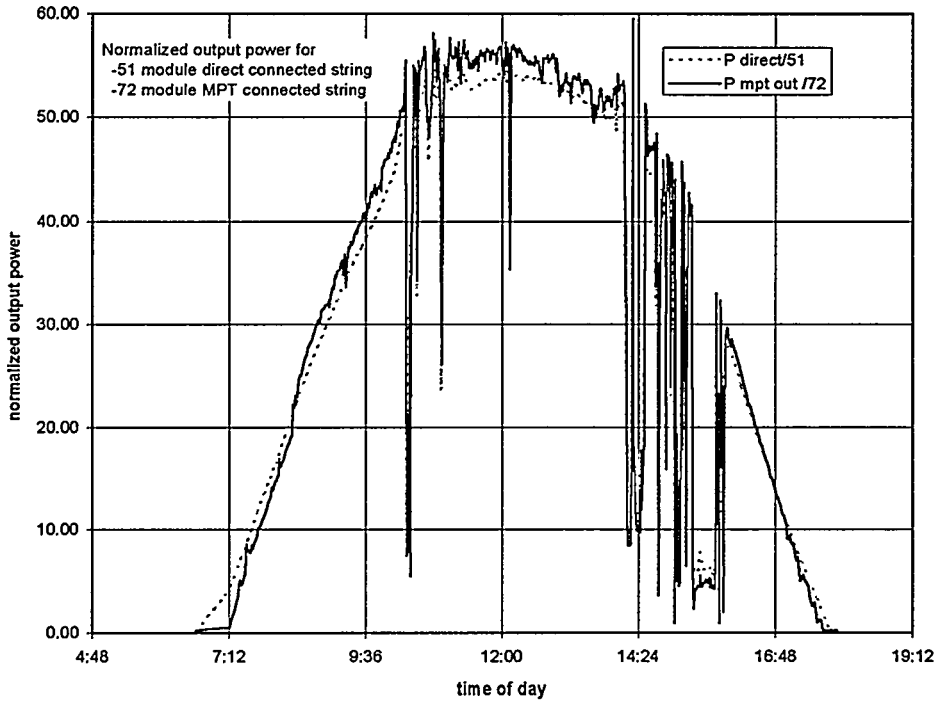

Figure 23: Normalized output power for direct and MPT connected strings

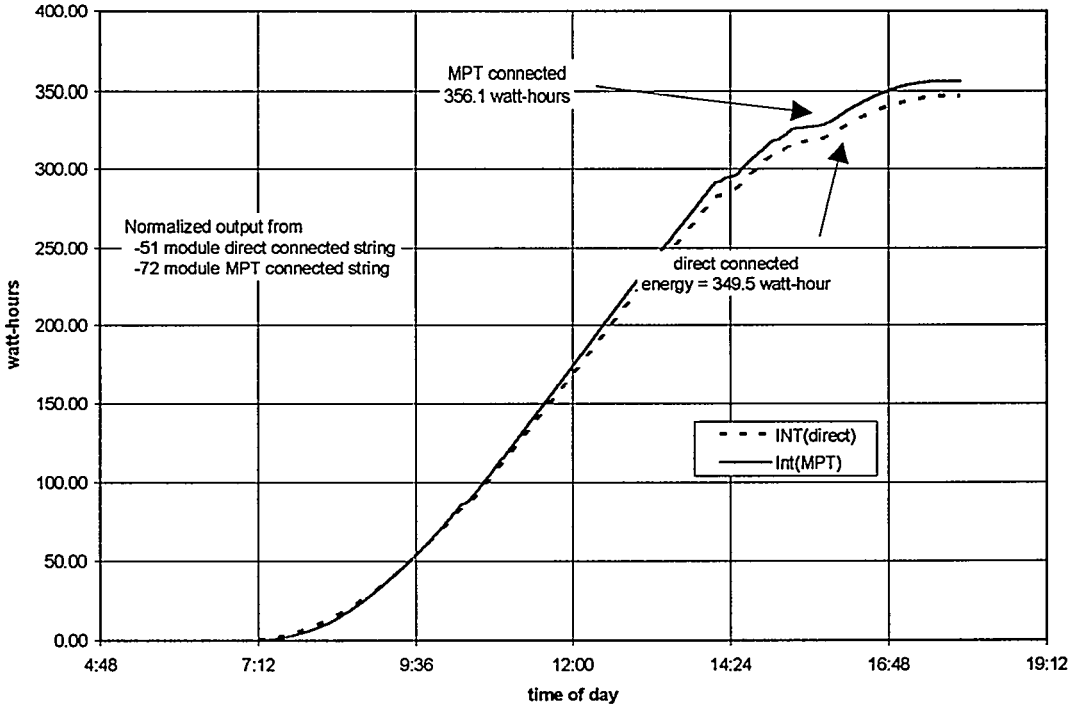

Figure 24: Comparison of direct connected and string connected modules

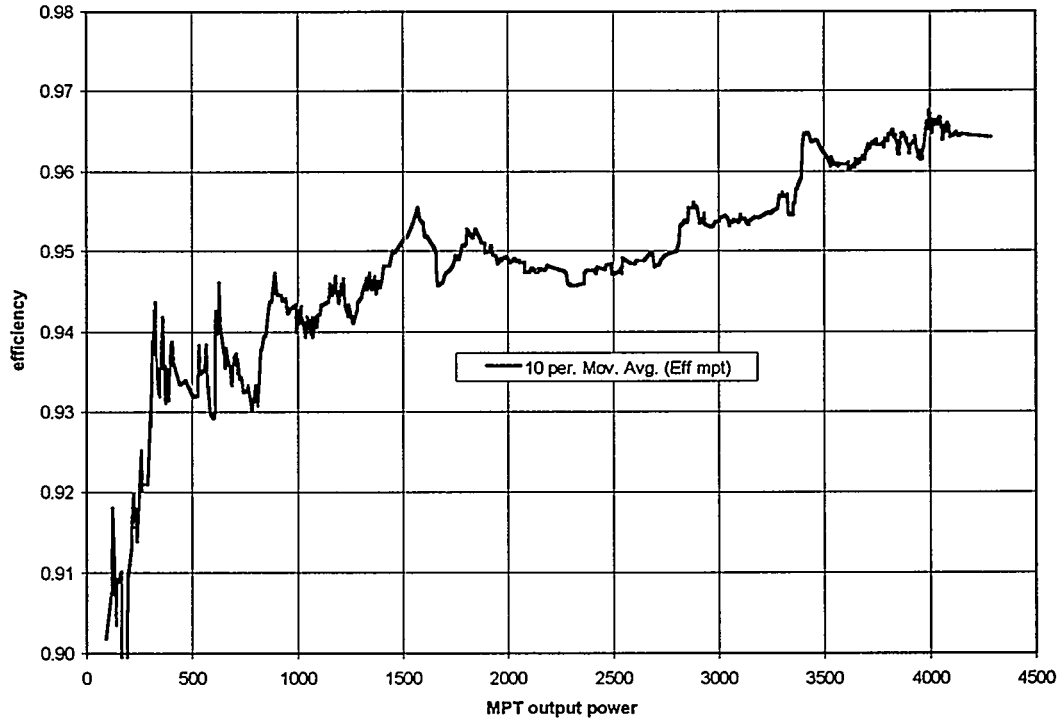

Figure 25: MPT efficiency of one 72 module string

3.2.7.3 Operating Limits.

The operating limits quantify the range of input voltages and peak power handling capability. Additionally, the MPT is designed to shut down to prevent overcharging of the battery. These values can be altered by changing firmware in future applications.

The input operating voltage can vary from 280 to 420 volts dc. This range of voltage was achieved from the array by running the test from dawn through solar noon.

Data.

The following functions were verified to operate as programmed in the Abacus firmware.

- The minimum start voltage is programmed to be 350 Vdc with a ten minute delay in turn on after reaching 350 Vdc.
- The MPT shutdown voltage is 280 Vdc.
- The MPT shut down when the battery voltage reached 219 Vdc.

4. References

1. Switching Power Converters, Page 235, Peter Wood, Van Nostrand Reinhold Company, 1981.
2 IEEE Std 1035-1989, "IEEE Recommended Practice: Test Procedure for Utility-Interconnected Static Power Converters."
3. "Performance and Characteristics of Inverters in Remote and Stand-Alone Applications," Ward Bower et. al., IEEE Twentieth PV Specialists Conference, 1988.
4. SAMS "Transformers and Motors," George Patrick Schultz, 1991, page 113.
5. IEEE c62.41-1991. "IEEE Recommended Practice on Surge Voltages in Low-Voltage AC Power Circuits.
6. IEEE C62.45-1992. "IEEE Guide on Surge Testing for Equipment Connected to Low-Voltage AC Power Circuits.

Appendix A: Measurement Matrix

Measurement matrix for Bimode® Tests			
SCXI Channel #	**Parameter**	**Bimode® Max Range**	**Bimode® Transd Model**
dc Signals			
1	Array Voltage Vpv	600	OSI VT7-12D
2	Array Current Ipv	120	Empro HA150-50 & OSI VT7-16D
3	MPT Output Current Impt	149	Empro HA150-50 & OSI VT7-16D
4	Bimode® total dc current Idc	196	Empro HA200-50 & OSI VT7-16D
5	Battery Voltage Vbat	338.4	OSI VT7-8D
6,7,8	Bimode® dc current per phase Idc(a,b,c)	74.3	Empro HA100-50 & OSI VT7-16D
9,10,11	Heat Sink Temperature T(a,b,c)		
Generator ac Signals			
12	Genset Phase A voltage Vg	304.7	Direct (FUSED)/YEW 2533 DPM #1
13	Genset Phase A current Iga	39.6	YEW 2241 Inst Xfmr/YEW 2533 DPM #1
14	Genset Phase A power Pga	11	YEW 2533 DPM #1 from 12 & 13
15	Genset Phase A Voltage Replica Vgarep	304.7	YEW 2533 DPM #1 from 12
16	Genset Phase A Current Replica Igarep	39.6	YEW 2533 DPM #1 from 13
17	Genset Phase B voltage Vg	304.7	Direct (FUSED)/YEW 2533 DPM #1
18	Genset Phase B current Igb	39.6	YEW 2241 Inst Xfmr/YEW 2533 DPM #1
19	Genset Phase B power Pgb	11	YEW 2533 DPM #1 from 17 & 18
20	Genset Phase B Voltage Replica Vgbrep	304.7	YEW 2533 DPM #1 from 17
21	Genset Phase B Current Replica Igbrep	39.6	YEW 2533 DPM #1 from 18
22	Genset Phase C voltage Vg	304.7	Direct (FUSED)/YEW 2533 DPM #1
23	Genset Phase C current Igc	39.6	YEW 2241 Inst Xfmr/YEW 2533 DPM #1
24	Genset Phase C power Pgc	11	YEW 2533 DPM #1 from 22 & 23
25	Genset Phase C Voltage Replica Vgcrep	304.7	YEW 2533 DPM #1 from 22
26	Genset Phase C Current Replica Igcrep	39.6	YEW 2533 DPM #1 from 23
27	Genset Avg Voltage Sigma Vg	304.7	YEW 2533 DPM #1 from 12, 17, & 22
28	Genset Avg Current Sigma Ig	120	YEW 2533 DPM #1 from 13, 18, & 23
29	Genset Total Power Sigma Pg	33	YEW 2533 DPM #1 from 14, 19, & 24

SCXI Channel #	Parameter	Bimode® Max Range	Bimode® Transd Model
Load ac Signals			
30	Load Phase A voltage Vla	304.7	Direct (FUSED)/YEW 2533 DPM #2
31	Load Phase A current Ila	39.6	YEW 2241 Inst Xfmr/YEW 2533 DPM #2
32	Load Phase A power Pla	11	YEW 2533 DPM #2 from 29 & 30
33	Load Phase A Voltage Replica Vlarep	304.7	YEW 2533 DPM #2 from 29
34	Load Phase A Current Replica Ilarep	39.6	YEW 2533 DPM #2 from 30
35	Load Phase B voltage Vlb	304.7	Direct (FUSED)/YEW 2533 DPM #2
36	Load Phase B current Ilb	39.6	YEW 2241 Inst Xfmr/YEW 2533 DPM #2
37	Load Phase B power Plb	11	YEW 2533 DPM #2 from 34 & 35
38	Load Phase B Voltage Replica Vlbrep	304.7	YEW 2533 DPM #2 from 34
39	Load Phase B Current Replica Ilbrep	39.6	YEW 2533 DPM #2 from 35
40	Loaed Phase C voltage Vlc	304.7	Direct (FUSED)/YEW 2533 DPM #2
41	Load Phase C current Ilc	39.6	YEW 2241 Inst Xfmr/YEW 2533 DPM #2
42	Load Phase C power Plc	11	YEW 2533 DPM #2 from 39 & 40
43	Load Phase C Voltage Replica Vlcrep	304.7	YEW 2533 DPM #2 from 39
44	Load Phase C Current Replica Ilcrep	39.6	YEW 2533 DPM #2 from 2240
45	Load Avg Voltage Sigma Vl	304.7	YEW 2533 DPM #2 from 29, 34, & 39
46	Load Total Current Sigma Il	120	YEW 2533 DPM #2 from 30, 35, & 40
47	Load Total Power Sigma Pl	33	YEW 2533 DPM #2 from 31, 36, & 41
Separately derived Time- & Freq-Resolved Signals to Rm 2 B/U Instrument (DSO, AA, DSA)			
48	Load Phase A Voltage Waveform Vlaw	304.7	Resistive Divider
49	Load Phase B Voltage Waveform Vlaw	304.7	Resistive Divider
50	Load Phase C Voltage Waveform Vlcw	304.7	Resistive Divider
51	Load Phase A Current Waveform Ilaw	39.6	Pearson 110A
52	Load Phase B Current Waveform Ilbw	39.6	Pearson 110A
53	Load Phase C Current Waveform Ilcw	39.6	Pearson 110A
54	Genset Phase A Voltage Waveform Vlaw	304.7	Resistive Divider
55	Genset Phase B Voltage	304.7	Resistive Divider

	Waveform Vlaw		
56	Genset Phase C Voltage Waveform Vlcw	304.7	Resistive Divider
57	Genset Phase A Current Waveform Ilaw	39.6	Pearson 110A
58	Genset Phase B Current Waveform Ilbw	39.6	Pearson 110A
59	Genset Phase C Current Waveform Ilcw	39.6	Pearson 110A

Appendix B: Terms and Definitions

Parameters are defined in this Appendix.

1. Total Harmonic Distortion (THD). Total harmonic distortion is the ratio of the rms value of the square root of the sum of the squared individual harmonic amplitudes to the rms value of the fundamental frequency of a complex waveform. This measurement does not include noise that occurs at nonharmonic frequencies. When specifying THD it is also necessary to specify the input voltage and the type and magnitude of the load. The waveforms should be analyzed for harmonic distortion at least to the 50th harmonic, or 3 kHz for a 60 Hz system. The proliferation of harmonic-rich loads on utility circuits, such as adjustable speed drives, lighting ballasts, computers, etc., has led to a stricter revised 1992 IEEE 519. Generally a spectrum analyzer is used to measure total harmonic distortion.

$$THD\ \%\ =\ \frac{\left[\left(H_1^2\right)\ +\ \left(H_2^2\right)+.\ .\ .\ .\ .\ .\ .+\left(H_n^2\right)\right]^{1/2}}{rms\ \ Fundamental}\ *\ 100\%$$

2 Total Distortion (TD). Total distortion is a measure of the difference between a pure sine waveform of a specified frequency and a test voltage waveform. TD is measured by an audio distortion analyzer. The audio analyzer filters out the fundamental frequency to obtain the numerator of the total distortion measurement. The measurement includes random noise and other repetitive phenomena, such as slip frequencies and not just the integer multiples of the fundamental frequency. Thus TD is always greater than or equal to THD.

$$TD\ \%\ =\ \frac{\text{noise}\ +\ \text{distortion}}{\text{signal}\ +\ \text{noise}\ +\ \text{distortion}}\ *\ 100\%$$

3 Power factor (pf). The ratio of true power to apparent power. It is primarily of interest because the allowable pf defines the reactive current the inverter must supply.

The pf can be measured for 3 cases, sinusoidal waveform, dist < 5%, and dist > 5%.

Case 1: Sinusoidal, pf = cos θ.

Case 2: Dist < 5%. pf = $P/(P^2 + Q^2)^{1/2}$ Where $(P^2 + Q^2)^{1/2}$ = apparent power (VA) and

Q = reactive power (VAR). This value reduces to Case 1 when the distortion is zero.

Case 3: Dist > 5%. Sometimes referred to as the rms power factor.

$$PF = \left(\frac{V_1 I_1 \cos\theta_1 + V_2 I_2 \cos\theta_2 + \cdots V_n I_n \cos\theta_n}{\left(V_1^2 + V_2^2 + \cdots V_n^2\right)\left(I_1^2 + I_2^2 + \cdots I_n^2\right)} \right)$$

where n is a whole integer multiplier of the fundamental frequency, 60 Hz. This expression is sometimes given as

$pf = W/(V_{rms} * I_{rms})$

where W is the real power. The accuracy of the power meter should be .025 pf for waveforms with < 5% THD.

4 Displacement Power Factor. The cosine of the displacement between the voltage and the current at the fundamental frequency.

5 Rated Power. The amount of power that can be continuously supplied to a resistive load at 25 degrees C. The power is applied until the unit reaches thermal equilibrium. The rated power may be a function of the dc input voltage.

6 Float Power/Tare Power. Power consumed by the inverter with no load.

7 Surge Power. The surge power, or peak power, is the amount of power that can be supplied to a transient load (such as a motor load) for seconds without interfering with normal inverter operation. The dc voltage input shall be within the manufacturer's specification range. The duration that peak power can be applied varies from manufacturer to manufacturer.

8 Efficiency. The inverter efficiency is the ratio of the output power to the average dc input power. The efficiency is a function of the dc input voltage, the load magnitude, and the load type.

9 Charger startup/shutdown thresholds. The set points for the charger to begin or stop battery charging at a preset value. It is dependent on the array output and battery parameters such as low-voltage disconnect (LVD), and high-voltage disconnect (HVD). This parameter only applies to inverters that include a battery charger.

10 Array Ripple Current. The variation in dc current amplitude in %; dc ripple current can cause power loss by changing the operating point on an array.

11 Voltage regulation. The stabilization of output ac voltage against fluctuations in source or load. For example, a single-phase nominal 120 Vac system operating voltages are: no less than 86.7%, no greater than 105.8%, and nominal operating voltage. Also see ANSI C84.1982.

12 Frequency stability. The ability of the inverter to provide a fixed 60 Hz output.

13 Transient Protection. The inverter should not fail as a result of electrical transients on either the dc or ac lines. No standards exist; however, goals can be established. A specification for transient immunity is described in IEEE C62.41-1991. Additionally, the inverter should survive short circuits that are on the load side of an ac fused disconnect (see Sand88-2974).

14 Electrical Shutdown. The inverter may be required to shutdown automatically if any of the following conditions occur:

a. Internal failure

b. Ground fault (generally refers to a fault > 5 mA for human safety. Will be amperes or more for most PV circuits.)

c. A power drain that could result in inverter damage.

15 Temperature. Generally the temperature of interest is the heat sync temperature. The inverter will operate with the specified inverter efficiency and maximum power levels during temperature cycling. The temperature was cycled throughout the allowable temperature range.

16 Radiated Emissions.

a. Acoustic noise. Acoustic noise is quantified by the decibel sound pressure level, dB spl. It is referenced to 20 micropascals of pressure. It is frequently weighted with an overlaid filter. The C filter is a linear filter that is standardized, while the A filter is an audible noise filter with a bandwidth of 500 to 5,000 Hz. For the purposes of a single noise reading in dB, the A filter was used. Spectral information, which may be valuable for identifying the source of the noise, was recorded with the C filter in use.

b. Electromagnetic Interference (EMI). EMI are electromagnetic radiation which causes interference with other equipment. Electrical emanations are examined to determine their compliance with FCC Title 47 of the Code of Federal Regulations, Part 15 "Radio Frequency Devices," Subpart J - "Computing Devices." The regulations apply to two classes of computing devices, Class A and Class B. A Class A device is marketed for use in a business/commercial/industrial area. A Class B device is marketed for use in a residential environment.

17 Maximum Power Tracking. The object of the maximum power tracker is to seek the maximum power possible from the array. There are two types. (1) Perturb and observe. The controlled variable is the array voltage. During each computation period, the array power is measured and compared to the power measurement from the computation period immediately preceding. If the new measurement exceeds or equals the old, the change in array voltage set point is in the same direction that previously caused the increase in power. If the new measurement is less than the old, the direction for the voltage set point change is reversed to seek an increase in array power. (2) The Derivative Method. Examine the derivative of power, which can be obtained by varying the voltage or current. Maximum power is achieved when the derivative is zero.

Distribution

George O'Sullivan
Abacus Controls, Inc.
P.O. Box 893
Somerville, NJ 08876-0893

Ron Matlin
Advanced PV (Photovoltaic) Systems
2300 North Wayney Way
Fairfield, CA 94533

Versyp Clois
Alaska Energy Authority
P.O. Box 190869
Anchorage, AK
99519-0869

Chris Fretas
Ananda Power Tech
14618 Tyler Foote Rd.
Nevada City, CA 95959

Tim Ball
Applied Power Corp.
1210 Homann Dr. SE
Lacey, WA 98503

Pete Eckert
Arizona Public Service Company
P.O. Box 53999
MS-4160
Phoenix, AZ 85072-3999

Bob Hammond
Arizona State University
CERS/CEAS
Tempe, AZ 85287-5806

Edward Kern
Ascension Technology
Box 314
Lincoln Center, MA. 01773

Allan Barnett
AstroPower, Inc.
Solar Park
Newark, DE 19716-2000

Bobier Electronics, Inc.
37th and Murdoch Ave.
Pakersburg, WV 26102

V. Vernon Risser
Daystar, Inc.
3240 Majestic Ridge
Las Cruces, NM 88011

Frank Goodman
Electric Power Research Institute
P.O. Box 10412
Palo Alto, CA 94303

Thomas Key
Electric Power Electronics Applications Center
10521 Research Dr., Suite 400
Knoxville, TN 37932

Chuck Whitaker
Endecon Engineering
3160 Crow Canyon Rd.
Suite 240
San Ramon, CA 94583

Alan Delahoy
EPV
P.O. Box 7456
Princeton, NJ 08543

Lane Garrett
ETA Engineering, Inc.
8502 Cactus Wren Road
Scottsdale, AZ 85250-4907

John Coors
Golden Photon
4545 McIntyre St.
P.O. Box 4040
Golden, CO 80403

Craig Brown
Heart Interface Corporation
21440 68th Ave. South
Kent, WA 98032-2416

Richard Perez
Home Power Magazine
P.O. Box 130
Hornbrook, CA 96044-0130

Gary Seifert
INEL (Id. Nat. Eng La)
2525 Fremont Ave.
P.O. Box 1625
Idaho Falls, ID 21702-3006

Michael Daugherty
Integrated Power Corp.
7618 Hayward Rd.
Frederick, MD 21702-3006

Bill Erdman
Kenetech
98 San Jacinto Blvd.
Suite 320
Austin, TX 78701

Martin Daub
Martin Marietta Corporation
Denver Division
Box 179
Denver, CO 80201

Mobile Solar Energy Corp.
4 Suburban Park Drive
Billerica, MA 01821

Ken Gerken
Morningstar Corp.
2911B
Olney Sandy Spring Rd.
Olney, MD 20832-1521

Lawrence Mott
Northern Power Systems
1 North Wind Road
Moretown, VT 05660-0659

Charlie Gay
National Renewable Energy Laboratory
1617 Cole Blvd.
Golden, CO 80401

Dick DeBlasio
National Renewable Energy Laboratory
1617 Cole Blvd.
Golden, CO 80401

Roger Taylor
National Renewable Energy Laboratory
1617 Cole Blvd.
Golden, CO 80401

Mike Crom
Naval Weapons Center
Code C02A1
China Lake, CA 93555-6001

Garyl Smith
Naval Weapons Center
Code C02A1
China Lake, CA 93555-6001

Robert Enterkine
Naval Air Warfare Center
Code C3206
China Lake, CA 93555

Hans Meyer
Omnion Power Electronics, Inc.
P.O. Box 879
2010 Energy Drive
East Troy, WI 53120-0879

Dave Porter
Omnion Power Electronics, Inc.
P.O. Box 879
2010 Energy Drive
East Troy, WI 53120-0879

Bob Schneider
Omnion Power Electronics, Inc.
P.O. Box 879
2010 Energy Drive
East Troy, WI 53120-0879

Brad Omara
Outside Power Consultants
1803 Aiskiyou
Klamath Falls, OR 97601

David Ross
Pacific Inverter, Inc.
509 Granite View Lane
Spring Valley, CA 92077

Greg Ball
Pacific Gas & Electric Co.
PV USA Project Office
2303 Camino Ramon
Suite 200
San Ramon, CA 94583

Brian Farmer
Pacific Gas & Electric Co.
PV USA Project Office
2303 Camino Ramon, Suite 200
San Ramon, CA 94583

Kevin L. Conlin
Photocomm, Inc.
13130 Stafford Road
Stafford, TX 77477

Robert Spotts
Photocomm, Inc.
7681 East Grey Road
Scottsdale, AZ 85260

Laurence Jennings
Photron, Inc.
P.O. Box 578
Willits, CA 95490-0578

Arthur Sams
Polar Products
2908 Oregon Court
Building K-4
Torrance, CA 90503

Paul Maycock
PV Energy Systems, Inc.
P.O. Box 290
Casanova, VA 22017

William Kaszeta
PV Resources, Int.
1440 W. Meseto Ave.
Mesa, AZ 85202

Clin Lashway
Raydec, Inc.
8210 La Mirada NE, Suite 700
Albuquerque, NM 87112

Len Loomans
Remote Power, Inc.
12301 North Grant St. #230
Denver, CO 80241-3130

Dave Collier
Sacramento Municipal Utility District
P.O. Box 15830
Sacramento, CA 95852-1830

Don Osborn
Sacramento Municipal Utility District
P.O. Box 15830
Sacramento, CA 95852-1830

J. Allen Gunn
Scientific Analysis, Inc.
6012 E. Shirley Lane
Montgomery, AL 36117

Keith Durand, Director
Solar Energy Industries Assn.
122 C Street NW, 4th Floor
Washington, DC 20001-2109

Scott Sklar
Solar Energy Industries Assn.
122 C Street NW, 4th Floor
Washington, DC 20001-2109

Raju Yenamandra
Siemens Solar, Inc.
4650 Adohr Lane
Camarillo, CA 93010

Rob Wills
Skyline Engineering
P.O. Box 134
Temple, NH 03084-0134

Steven Strong
Solar Design Associates
P.O. Box 242
Harvard, MA 01451-0242

Paul McClusky
Solar Electric Specialities
P.O. Box 537
Willits, CA 95490

Neil Kaminar
Solar Engineering Applications
3500 Thomas Rd., Suite E
Santa Clara, CA 95054

Johnny Weiss
Solar Technology Institute
P.O. Box 715
Carbondale, CO 81623-0715

Ramon Dominguez
Solarex Corp.
630 Solarex Ct.
Fredrick, MD 21701

Steven Durand
Southwest Technical Development Institute
P.O. Box 30001, Dept. 3SOL
Las Cruces, NM 88003-0001

John Wiles
Southwest Technical Development Institute
P.O. Box 30001
Dept. 3SOL
Las Cruces, NM 88003-0001

Tom Philp
Specialty Concepts, Inc.
8954 Mason Ave.
Chatsworth, CA 91311-6107

James Beck
Systems Research Group
10151 University Blvd.
Suite 171
Orlando, FL 32817

Tom Lundviet
Texas Instuments
P. O. Box 655012
Dallas, TX 75265

Ray Barbee
Trace Engineering Company
5916 195th St. NE
Arlington, WA 98223

Arthur Rudin
Translumin
101 Willow St.
Franklin, LA 70538-6135

Larry Slomenski
United Solar Systems Corp.
5728 Eastgate Mall
San Diego, CA 92121-2814

Dr. Ned Mohan
Professor of Electrical Engineering
University of Minnesota
200 Union St. SE
Minneapolis, MN 55455

Bud Annan
U.S. Department of Energy
Forrestal Building, EE-13
1000 Independence Avenue SW
Washington, DC 20585

Alec Bulawka
U.S. Department of Energy
Forrestal Building, EE-131
1000 Independence Avenue SW
Washington, DC 20585

Mike Pulscak
U.S. Department of Energy
Forrestal Building, EE-131
1000 Independence Avenue SW
Washington, DC 20585

Jim Rannels
U.S. Department of Energy
Forrestal Building, EE-131
1000 Independence Avenue SW
Washington, DC 20585

Mike Davis
U.S. Department of Energy
Forrestal Building, Room 8G-033
1000 Independence Avenue SW
Washington, DC 20585

Mike Stern
Utility Power Group
9410 DeSoto Ave. , Unit G
Chatsworth, CA 91311-4947

Rick West
Utility Power Group
4444 Orcutt Rd.
San Luis Obispo, CA 93401

Wattsun Corp.
B14 2nd St. SW
Albuquerque, NM 87103

David Goeser
Westinghouse Electric Corp.
Advanced Energy Systems Division
P.O. Box 355
Pittsburg, PA 15230

SANDIA DISTRIBUTION

0613	G.P. Corey, 2225
0702	D.E. Arvizu, 6200
0702	A. VanArsdall, 6200
0753	C.P. Cameron & Staff, 6218
0752	M.L. Tatro & Staff, 6219
0703	C.E. Tyner, 6216
1127	J.M. Chavez, 6215
0899	Technical Library, 13414 (5)
0619	Print Media, 12615
0100	Document Processing for DOE/OSTI, 7613-2 (5)
9018	Central Technical Files, 8523-2